Thermochemistry of small cationic iron–sulfur clusters

Konrad Koszinowski, Detlef Schröder, and Helmut Schwarz
Institut für Chemie der Technischen Universität Berlin, Straße des 17. Juni 135, D-10623 Berlin, Germany

Rohana Liyanage and P. B. Armentrout
Department of Chemistry, University of Utah, Salt Lake City, Utah 84112

(Received 11 July 2002; accepted 10 September 2002)

The kinetic energy dependences of the reactions of Fe_n^+ with COS ($n=2-6$) and CS_2 ($n=2-5$) are studied in a guided-ion beam tandem mass-spectrometer. The main products arise from sulfur transfer and subsequent losses of Fe atoms. In the case of CS_2, this reactant also formally replaces one Fe atom of the cluster to form $Fe_{n-1}CS_2^+$ with losses of further Fe atoms at elevated energies. In addition, the kinetic energy dependences of the reactions of Fe_nS^+ ($n=2-4$) with Xe and CS_2 are studied. The former system yields collision-induced dissociations, whereas the latter reagent effects sulfur transfer accompanied by subsequent losses of Fe atoms. Analyses of the cross sections for endothermic reactions yield the bond energies $D_0(Fe_n^+-S)$, $n=2-5$, $D_0(SFe_{n-1}^+-Fe)$, $n=2-5$, $D_0(SFe_n^+-S)$, $n=1-3$, and $D_0(S_2Fe_{n-1}^+-Fe)$, $n=2, 3$, as well as the ionization energy $IE(Fe_2S_2)$. These values are derived with explicit consideration of the lifetimes of the energized reaction intermediates. The binding between sulfur and the cluster core strengthens as the cluster size increases, which is rationalized by simple structural arguments. © *2002 American Institute of Physics.* [DOI: 10.1063/1.1518004]

I. INTRODUCTION

Iron–sulfur clusters are certainly among the most fascinating transition-metal species found in biological systems. Their appeal arises from the combination of structural simplicity, in the eyes of a chemist even beauty, with their importance in numerous biological processes. Nature has chosen iron–sulfur clusters like [2Fe–2S], [3Fe–4S], [4Fe–4S], and the FeMo cofactor of nitrogenase as active centers in the so-called ferredoxins, proteins crucially involved in electron-transfer reactions occurring in photosynthesis, respiration, and nitrogen fixation.[1–4] Besides the pivotal role in biological redox processes, iron–sulfur clusters are increasingly recognized to catalyze dehydration reactions, to regulate metabolic pathways, to act as biological sensors (for Fe, O_2, and O_2^-), and to stabilize protein structures.[5]

The great progress made in the characterization of biogenous iron–sulfur clusters in the last decades was only possible thanks to truly interdisciplinary efforts of biology, biochemistry, spectroscopic, and diffractometric methods. However, understanding the chemistry of these species does not only require knowledge of their structures, but also of their energetics.

The determination of thermochemical data of size-selected metal clusters lies largely in the domain of gas-phase techniques. These methods probe intrinsic properties of the species under investigation while deliberately avoiding the complicating influences of counterions, ligands, and solvents. Thus, the experimental results are directly comparable with data obtained in theoretical studies. Concerning iron–sulfur clusters, the thermochemical knowledge is still rather limited. Photoelectron spectroscopy of the anionic clusters $Fe_nS_m^-$ ($n, m=1-6$) provided electron affinities and vertical detachment energies.[6,7] For FeS, the first and second ionization energies (IEs) were determined by different mass spectrometric methods and *ab initio* calculations.[8] Mass spectrometric investigations also provided the ionization energy of FeS_2.[9] Several experimental studies have obtained bond-dissociation energies (BDEs) for FeS_m^+,[9–11] but only little information is available for clusters with more than one iron atom.[12] However, recent theoretical work investigated the thermochemical properties of the $Fe_2S^{+/0/-}$ and $Fe_2S_2^{+/0/-}$ species.[13,14] The relative stabilities of the clusters $Fe_nS_m^{+/0/-}$ are of particular interest because there might exist a correlation with their biological activity. Indeed, the relative abundance of both cationic and anionic clusters produced by laser-vaporization sources indicates an enhanced stability for $n \approx m$.[6,15–17] If this finding were valid for physiological media as well, one could speculate that nature's usage of iron–sulfur clusters in biological systems might not only have been driven by their special structural and electronic features but also by a comparatively ready availability. Such conclusions may be important, considering that iron–sulfur clusters have been assigned a central role in the evolution of life.[18–20]

A particularly valuable tool in ion thermochemistry is the guided ion beam (GIB) tandem mass spectrometry technique.[21–23] It has been successfully applied in the thermochemical characterization of cationic iron clusters Fe_n^+ themselves[24,25] and some of their derivatives.[26–29] Equally important, it has also been used to determine the BDEs of FeS^+ and FeS_2^+ by measuring the reaction enthalpies of sulfur transfer from carbon disulfide, CS_2, to Fe^+ and FeS^+, respectively.[9] These results fully agreed with equilibrium measurements performed in a Fourier transform ion-cyclotron resonance mass-spectrometer.[9]

The present work aims to extend our previous studies of mononuclear iron sulfides to small cationic iron clusters. It

has already been shown that iron–sulfur clusters $Fe_nS_m^+$ are formed by the reaction of Fe_n^+ with CS_2 in the gas phase.[17] Here, such sulfur–transfer reactions are used to determine iron–sulfur BDEs, applying both COS and CS_2 as sulfur-transfer reagents. Additionally, the collision-induced dissociation (CID) of Fe_nS^+ clusters is investigated.

II. EXPERIMENTAL DETAILS

The ion beam apparatus used in this work has been described in detail elsewhere.[30] The formation of bare iron-cluster cations Fe_n^+ is achieved by laser vaporization/ionization and ensuing supersonic expansion.[31] Briefly, a copper vapor laser (Oxford ACL-35, 511 and 578 nm, 8 kHz repetition rate, 3–4 mJ/pulse) is focused onto a rotating and translating iron rod (cold-rolled steel). The plasma thus created is entrained in a continuous flow (5000–6000 sccm) of helium. Clustering of the iron atoms and ions occurs in a 2 mm diam and 63 mm long condensation tube immediately following the target where the ions undergo approximately 10^5 collisions with He atoms. The gas mixture then expands into a field-free region and is skimmed. The expansion further cools the internal modes of the clusters so that these are assumed to be thermalized to 298 K.[24,32,33] The generation of binary cluster ions $Fe_nS_m^+$ occurs in basically the same way when CS_2 is added to the He flow. For achieving a sufficient and steady intensity of binary cluster ions, careful control of the partial pressure of CS_2 is very important.

The positively charged ions are extracted from the source, injected into a magnetic sector-momentum analyzer, decelerated to a desired kinetic energy, and focused into a radio-frequency (rf) octopole ion-guide.[34,35] A section of the octopole is surrounded by the reaction cell where the neutral gas (COS or CS_2 for sulfur-transfer reactions and Xe for CID) is introduced. The pressure of the neutral reagent is kept relatively low (≈1–20 mPa) to reduce the probability of multiple collisions. For excluding or probing such multiple collisions, all reactions studied were conducted at two or more different pressures of the neutral reactants. While being trapped in the steep radial potential well created by the rf electric fields, the product and remaining reactant ions drift to the end of the octopole. The ions then are extracted and injected into a quadrupole mass filter for mass analysis. Finally, the ion intensities are measured with a Daly detector[36] coupled with standard pulse counting techniques. Reactant-ion intensities used in this work were typically $0.2–1.0 \times 10^6$ ions s^{-1}. Observed product-ion intensities are converted to absolute reaction cross sections on the basis of the 4π collection characteristics of the octopole, as detailed elsewhere.[37] Absolute errors in the cross sections are estimated at approximately 30%.

CID experiments were performed to verify the identity of the ionic reactants and to ensure the absence of any excessive internal excitation. The former especially proved necessary in the case of the binary $Fe_nS_m^+$ cluster ions because of isobaric interferences. For instance, setting the magnetic sector-momentum analyzer at the nominal mass of $Fe_2S_2^+$, $m/z=176$, the CID products indicated the presence of both the desired $Fe_2S_2^+$ ions and $[Fe,C_2,S_3]^+$, because $m(Fe)=m(C_2,S)$. Analogous interferences continue for larger clusters, so only binary reactant ions containing a single sulfur atom, Fe_nS^+, were further investigated. For these, the absence of the isobaric dioxides, $Fe_nO_2^+$, had also to be ensured. To this end, $Fe_4O_2^+$ was produced deliberately by adding oxygen instead of CS_2 to the He flow. The CID spectra of both $Fe_4O_2^+$ and Fe_4S^+ were compared at $m/z=128$, which can be unambiguously assigned to Fe_2O^+. From the ratio of cross sections, the presence of 2% $Fe_4O_2^+$ in the Fe_4S^+ beam was inferred. For Fe_2S^+ and Fe_3S^+, similarly small contaminations were assumed and considered negligible in the further analysis.

Data collection for each reaction system was repeated several times to ensure reproducibility of results. The absolute zero in the kinetic energy scale of the ions and their Gaussian shaped energy distributions were measured using the octopole as a retarding energy analyzer.[37] The full width at half maximum of the distributions varied with cluster size from 0.7 to 1.0 eV. The uncertainty in the absolute energy scale is ±0.05 eV (lab). Kinetic energies in the laboratory frame (lab) are converted to energies in the center-of-mass (CM) frame according to the stationary target approximation

$$E(\mathrm{CM})=E(\mathrm{lab})\times M/(M+m), \tag{1}$$

where M and m are the masses of the neutral and ionic reactants, respectively.[37] Unless stated otherwise, all energies quoted in the following correspond to the CM frame.

III. DATA ANALYSIS

The quantitative analysis of the energy dependence of reaction cross sections $\sigma(E)$ utilizes Eq. (2),

$$\sigma(E)=\sigma_0\sum_i g_i(E+E_i-E_0)^N/E, \tag{2}$$

where E is the relative collision energy, E_0 is the reaction threshold at 0 K, σ_0 is an energy independent scaling factor, and N is an adjustable parameter ($N=1$ in the limit of hard sphere collisions) that describes the energy deposition distribution.[38] The summation is over the rovibrational states of the reactants having energies E_i and populations g_i, where $\Sigma g_i=1$. The relative reactivities of all rovibrational states, as reflected by σ_0 and N, are assumed to be equivalent. The Beyer–Swinehart algorithm is used to evaluate the density of rovibrational states,[39–41] and the relative populations g_i are calculated according to Maxwell–Boltzmann distributions.

For metal clusters, lifetime effects become important as the cluster size increases and have to be explicitly treated for the extraction of accurate thermochemical data from threshold experiments.[21,22,42,43] Because of the high number of easily accessible rovibrational states, energy redistribution in the transient intermediate is assumed to be very effective. Hence, the lifetime of the metastable intermediate, the so-called energized molecule (EM), can exceed the experimental time window τ (about 10^{-4} s in the apparatus used) available to the reaction. This results in a kinetic shift of the experimental threshold towards energies higher than the thermochemical endothermicity. To statistically account for this phenomenon,

the Rice–Ramsperger–Kassel–Marcus (RRKM) theory[44–46] is incorporated into Eq. (2). For simple CID reactions, this yields Eq. (3),[47]

$$\sigma(E)=\sum_i g_i(N\sigma_0/E)\int_0^{E_T-E_0}(\Delta E)^{N-1}\times[1-e^{-k(E_T-\Delta E)\tau}]\mathrm{d}(\Delta E). \quad (3)$$

Here, $E_T=E+E_i$ is the total energy available to the reactants, ΔE is the energy remaining in translation after the collision between the reactants, $k(E_T-\Delta E)$ is the unimolecular rate constant, and all other parameters are the same as in Eq. (2). Defining the internal energy of the EM, $E^*=E_T-\Delta E$, the unimolecular rate constant $k(E_T-\Delta E)=k(E^*)$ is given as

$$k(E^*)=sN^{\dagger}_{\nu,r}(E^*-E_0)/h\rho_{\nu,r}(E^*), \quad (4)$$

where s is the reaction degeneracy[44,46] (in this work, s is assumed to equal the cluster size n for the reactions of interest), $N^{\dagger}_{\nu,r}(E^*-E_0)$ is the sum of rovibrational states of the TS at an energy E^*-E_0 above the dissociation energy E_0, h is Planck's constant, and $\rho_{\nu,r}(E^*)$ is the rovibrational density of states of the EM at the energy available, E^*. A modification of this approach to account for slightly more complex reaction mechanisms is discussed below.

After convoluting both the kinetic energy distribution of the ion beam and the thermal motion of the neutral target gas into Eq. (2) or (3), the model is compared to the experimental data. To this end, σ_0, N, and E_0 are optimized to best reproduce the experimental cross sections using a least squares criterion. The model applied explicitly accounts for the rovibrational energy of the reactants and includes the assumption that all of the internal energy is capable of coupling into the reaction coordinate. The thresholds derived from modeling the experimental data therefore correspond to the formation of products with no internal excitation, i.e., with an effective temperature of 0 K.

The model neglects possible electronic excitations. These may be present in the case of transition-metal clusters which are assumed to possess a manifold of different electronic states with low energy spacings. The effects of such electronic excitations on CID thresholds have scarcely been investigated. Shvartsburg *et al.* addressed the incorporation of electronic degrees of freedom into RRKM theory to describe the unimolecular decomposition of metal clusters.[48] Basically, they find that extending the system's density of states reduces the unimolecular rate constant and, thus, enlarges the kinetic shift of the energy threshold because accumulation of the required energy in the reaction mode becomes less probable. However, this effect appeared to be small for clusters M_n^+ with $n\leqslant 10$. In the photodissociation of Al_{10}^+, for example, consideration of electronically excited states causes the threshold to shift by $\Delta E_0^{el}=0.02$ eV.[48] Therefore, neglecting excited electronic states is assumed not to appreciably affect the threshold analysis of the present experiments.

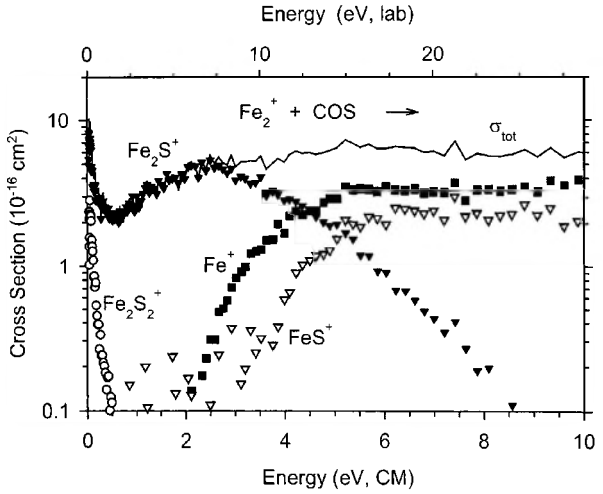

FIG. 1. Main-product cross sections for the reaction of Fe_2^+ with COS as a function of center-of-mass energy (lower axis) and laboratory energy (upper axis). $Fe_2S_2^+$ is formed via multiple collisions.

IV. RESULTS

A. Qualitative analysis of cross sections

The reactions of Fe_n^+ with COS ($n=2-6$) and with CS_2 ($n=2-5$) as well as the reactions of Fe_nS^+ ($n=2-4$) with Xe and with CS_2 were studied varying the kinetic energies from 0 to about 10 eV in the center-of-mass frame. The corresponding reactions of Fe^+ and FeS^+ with COS and CS_2 have already been reported in the literature.[9,49]

1. Reactions of Fe_n^+ with COS

The reaction of Fe_2^+ with COS leads to Fe_2S^+ as the main cationic product over an energy range from 0.2 to 4 eV in reaction (5),

$$Fe_2^+ + COS \rightarrow Fe_2S^+ + CO. \quad (5)$$

This seemingly simple sulfur transfer clearly shows a bimodal shape (Fig. 1). At low energies, the declining cross section indicates an exothermic reaction and thus that $D_0(Fe_2^+-S)>D_0(OC-S)=3.14$ eV (Table I).[50,51] At about 0.7 eV, the cross section starts to rise, which implies that a second pathway is operative. Composite cross sections could arise from the involvement of different structural isomers or electronic states of reactants or products as well as competing reaction mechanisms. However, because bimodal behavior is also observed in the analogous reactions of larger Fe_n^+

TABLE I. Bond dissociation energies (BDEs) of Fe_n^+, $FeCS^+$ and CXS (X=O, S).

Bond	D_0/eV[a]	Bond	D_0/eV[b]
Fe^+–Fe	2.78±0.10	Fe^+–CS	2.40±0.12[c]
Fe_2^+–Fe	1.75±0.12		
Fe_3^+–Fe	2.23±0.20	OC–S	3.140±0.005
Fe_4^+–Fe	2.70±0.23	SC–O	6.88±0.04
Fe_5^+–Fe	3.27±0.25	SC–S	4.50±0.04

[a]References 24, 25.
[b]Reference 49.
[c]Reference 9.

clusters with COS and CS_2 (see below) as well as CO_2,[28] a rather general origin that is basically independent of the very nature of the metal center appears plausible. The dissociation of CXY ($^1\Sigma$) species (X, Y=O, S) can provide products differing in their electronic states according to reactions (6a) and (6b),

$$CXY(^1\Sigma) \rightarrow CX(^1\Sigma) + Y(^3P). \quad (6a)$$

$$\rightarrow CX(^1\Sigma) + Y(^1D). \quad (6b)$$

Reaction (6a) yields products in their electronic ground states and, thus, is the energetically less demanding process but requires spin-inversion which may reduce its efficiency. Such a restriction does not exist for reaction (6b) so that this process should be favored once sufficient energy is provided (the $^3P-^1D$ splitting of atomic sulfur amounts to 1.15 eV).[52] Although the situation is presumably more complicated in the presence of a metal center, reactions (6a) and (6b) may still serve to describe the basic features.

At about 2.5 eV, the cross section of Fe_2S^+ starts to decline again while simultaneously the ionic products Fe^+ and FeS^+ emerge and the total cross section remains constant at about 7 Å^2. Obviously, Fe_2S^+ formed at this energy is no longer stable and decays in secondary reactions, reactions (7a) and (7b), respectively,

$$Fe_2^+ + COS \rightarrow Fe_2S^+ + CO \rightarrow Fe^+ + FeS + CO \quad (7a)$$

$$\rightarrow FeS^+ + Fe + CO. \quad (7b)$$

The formation of neutral FeS, which has a bond energy of 3.31 ± 0.15 eV,[53] rather than of separated Fe and S atoms can be safely inferred from thermochemical considerations as the latter products cannot be formed until 5.92 ± 0.10 eV (Table I). The threshold of the Fe^+ channel rises earlier than that of FeS^+, in agreement with the higher ionization energy of FeS (IE(FeS)$=8.3 \pm 0.3$ eV) (Ref. 8) compared to Fe (IE(Fe) $=7.90$ eV).[54] With respect to the neutral products concomitant with the latter, bond formation between Fe and CO is also possible; however, because of the high effective temperature in the transient energized molecule (EM), loss of the weakly bound FeCO species [D_{298}(Fe–CO)$=0.35 \pm 0.15$ eV,[55] 0.46 ± 0.16 eV (Ref. 56)] rather than separated Fe and CO appears unlikely. Note that Fe^+ may also result from simple CID of Fe_2^+ above 2.78 ± 0.10 eV.

Fe_2O^+ is another product formed from the Fe_2^+/COS system, reaction (8),

$$Fe_2^+ + COS \rightarrow Fe_2O^+ + CS. \quad (8)$$

The oxygen transfer is endothermic and less efficient than its sulfur counterpart by more than two orders of magnitude with a maximum cross section of $\sigma_{max}(Fe_2O^+) \approx 0.04$ Å^2 (off scale in Fig. 1) and an apparent threshold of $E_0 \approx 2.0$ eV. This simply reflects the difference in the two different BDEs of COS (Table I).

In contrast to the products formed in reactions (5), (7) and (8), the $Fe_2S_2^+$ ion (Fig. 1) is attributed to the occurrence of multiple collisions, which manifest themselves in a marked pressure dependence of the product's cross section. Its steeply falling shape further suggests that the reaction, $Fe_2S^+ + COS \rightarrow Fe_2S_2^+ + CO$, is exothermic. The notable interference of the termolecular $Fe_2S_2^+$ product also implies that this second sulfur transfer from COS to the Fe_2^+ cluster is faster than the first one, reaction (5).

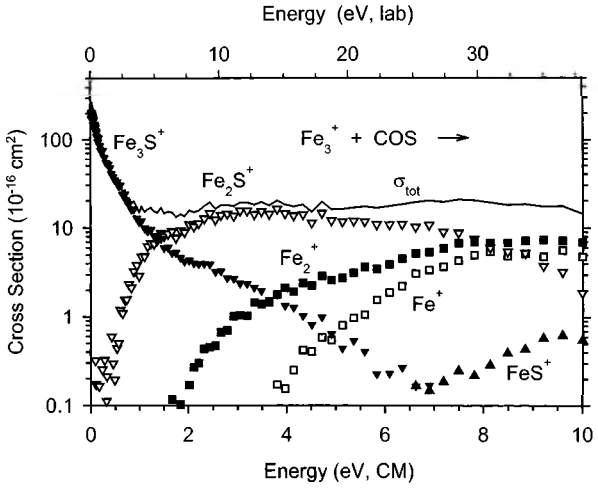

FIG. 2. Main-product cross sections for the reaction of Fe_3^+ with COS as a function of center-of-mass energy (lower axis) and laboratory energy (upper axis). For minor products observed, see text.

The reaction between Fe_3^+ and COS results in a primary sulfur transfer, reaction (9),

$$Fe_3^+ + COS \rightarrow Fe_3S^+ + CO, \quad (9)$$

which is exothermic like in the case of Fe_2^+ but much more efficient (Fig. 2). Careful inspection of the product's cross section shows that its decrease does not follow a simple power law as one would generally expect for an exothermic reaction but that its negative slope almost vanishes about 2 eV. This behavior might indicate the presence of a second, endothermic process like in the case of reaction (5). The data are consistent with such a process having a similar magnitude as that of the Fe_2^+/COS system, but are obscured by the much more efficient exothermic channel in the Fe_3^+/COS system. The Fe_2S^+ ion is assigned to be a secondary product stemming from the decay of the primary Fe_3S^+ product [reaction (10)],

$$Fe_3^+ + COS \rightarrow Fe_3S^+ + CO \rightarrow Fe_2S^+ + Fe + CO. \quad (10)$$

Fe_2^+ results from simple CID as the apparent threshold of this channel is in agreement with $D_0(Fe_2^+ - Fe) = 1.75 \pm 0.12$ eV (Table I). From the Fe_2^+/COS system, the Fe^+ and FeS^+ ions are already known as dissociation products of Fe_2S^+ having excess energy. Thus, these species are termed as tertiary products formed in reactions (11a) and (11b), respectively,

$$Fe_3^+ + COS \rightarrow Fe_3S^+ + CO \rightarrow Fe_2S^+ + Fe + CO$$

$$\rightarrow Fe^+ + FeS + Fe + CO \quad (11a)$$

$$\rightarrow FeS^+ + 2Fe + CO. \quad (11b)$$

Again, the formation of Fe^+ is favored compared to that of FeS^+. At energies higher than $D_0(Fe_2^+ - Fe) + D_0(Fe^+ - Fe) = 4.53 \pm 0.16$ eV (Table I), Fe^+ can also result from simple CID of Fe_3^+, a process that presumably contributes to the relative magnitude of the Fe^+ cross section. The only product arising from oxygen transfer is Fe_2O^+. Its formation is endothermic and not efficient [$\sigma_{max}(Fe_2O^+) \approx 0.6$ Å^2, omit-

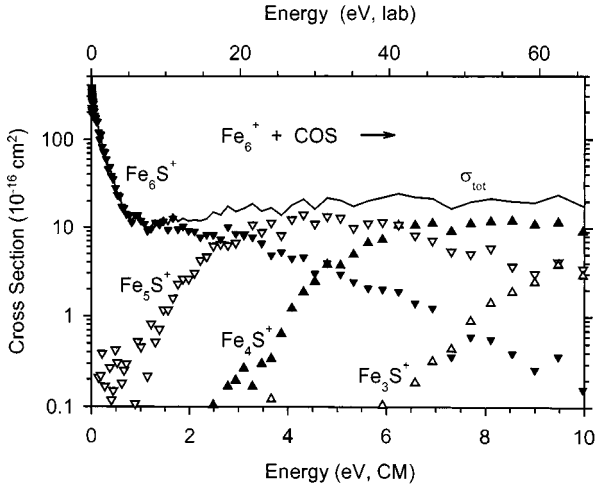

FIG. 3. Main-product cross sections for the reaction of Fe_6^+ with COS as a function of center-of-mass energy (lower axis) and laboratory energy (upper axis). For CID and minor products observed, see text.

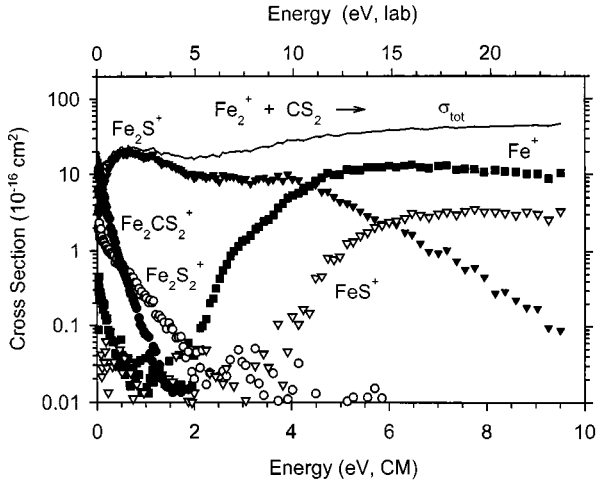

FIG. 4. Product cross sections for the reaction of Fe_2^+ with CS_2 as a function of center-of-mass energy (lower axis) and laboratory energy (upper axis). $Fe_2CS_2^+$ and $Fe_2S_2^+$ are formed via multiple collisions.

ted in Fig. 2, apparent threshold ≈3.0 eV]. At low energies, $Fe_2S_2^+$, $Fe_3S_2^+$, and $Fe_3S_3^+$ are also observed and show pressure dependent cross sections, confirming their formation in multiple collisions (omitted in Fig. 2). In all cases, these cross sections show no obvious barriers, suggesting that each of these consecutive reactions is therefore almost certainly exothermic.

The Fe_n^+/COS systems, $n=4-6$, resemble each other very much. The primary sulfur-transfer reactions (12) ($x=0$),

$$Fe_n^+ + COS \rightarrow Fe_{n-x}S^+ + xFe + CO. \quad (12)$$

are exothermic and show varying degrees of composite behavior (exemplified in Fig. 3 for $n=6$), *i.e.*, both exothermic reactivity as well as a cross section feature at higher energies that can be assigned to a kinetically favored, but endothermic process. At elevated energies, successively secondary and tertiary reactions occur, reaction (12) with $x=1$ and 2, respectively. For Fe_5^+ and Fe_6^+, even the formally quaternary products yielding $Fe_{n-3}S^+$ are observed, reaction (12) with $x=3$. The different channels have approximately equidistant thresholds, clearly suggesting sequential losses of Fe atoms.

The secondary sulfur-transfers, reaction (12) with $x=1$, show small nonzero cross sections at thermal energies (Fig. 3). These tails cannot arise from reactions with O_2 as a contaminant, because other products would have been seen and the energy dependences of the cross sections observed would have been different (see below). Instead, the tails might indicate the presence of small amounts of excited Fe_n^+ ions having sufficient energy to undergo these reactions at thermal energies. Prior to threshold analyses, these tails were fitted and subtracted from the measured cross sections.

Oxygen transfers from COS result in the endothermic formations of $Fe_{n-1}O^+$ and $Fe_{n-2}O^+$ with low efficiencies ($\sigma_{max}<0.5$ Å^2). Additionally, CID products (Fe_{n-x}^+, $x=1-3$ for $n=4$ and $x=1,2$ for $n=5,6$) are observed, along with exothermic formation of products resulting from multiple collisions. In the Fe_4^+/COS system, for example, $Fe_4S_2^+$, $Fe_4S_3^+$, $Fe_4S_4^+$, $Fe_3S_2^+$, and $Fe_3S_3^+$ show strongly pressure dependent cross sections.

2. Reactions of Fe_n^+ with CS_2

The reactions observed in the Fe_2^+/CS_2 system are closely related to those occurring between Fe_2^+ and COS. Again, Fe_2S^+ is the main product observed over an energy range from 0.2 to 4 eV (Fig. 4). However, its rising cross section at low energies indicates a slightly endothermic primary sulfur transfer, reaction (13),

$$Fe_2^+ + CS_2 \rightarrow Fe_2S^+ + CS. \quad (13)$$

This different behavior reflects the higher C–S bond strength of CS_2 compared to COS and provides an upper limit for the BDE of Fe_2S^+ according to $D_0(Fe_2^+-S)<D_0(SC-S)=4.50\pm0.04$ eV (Table I). At medium energies (2–4 eV), the second feature comparable to that observed in the Fe_2^+/COS system contributes to the Fe_2S^+ channel. Above 4 eV, the Fe_2S^+ cross section declines giving way to the secondary products Fe^+ and FeS^+, respectively. The Fe^+ channel emerges before the Fe_2S^+ cross section begins to decline, a result that is attributed to simple CID at energies above $D_0(Fe^+-Fe)=2.78\pm0.10$ eV (Table I). At energies below 1 eV, the Fe^+ cross section shows yet another, rather minor feature whose energy dependence indicates an exothermic process. However, no substantially exothermic reaction between Fe_2^+ and CS_2 yielding Fe^+ seems feasible. Further CID experiments employing Xe as collision gas excluded the presence of electronically excited Fe_2^+ in the ion beam. Thus, the exothermic Fe^+ feature is tentatively ascribed to the reaction of Fe_2^+ with residual O_2 in the collision volume, a process known to exothermically give rise to Fe^+ and neutral FeO_2.[57] From the known cross section of this reaction at thermal energies,[57] the O_2 fraction in the present experiment can be estimated at ≤0.3%. This value is low enough to not affect the cross sections of the other reactions.

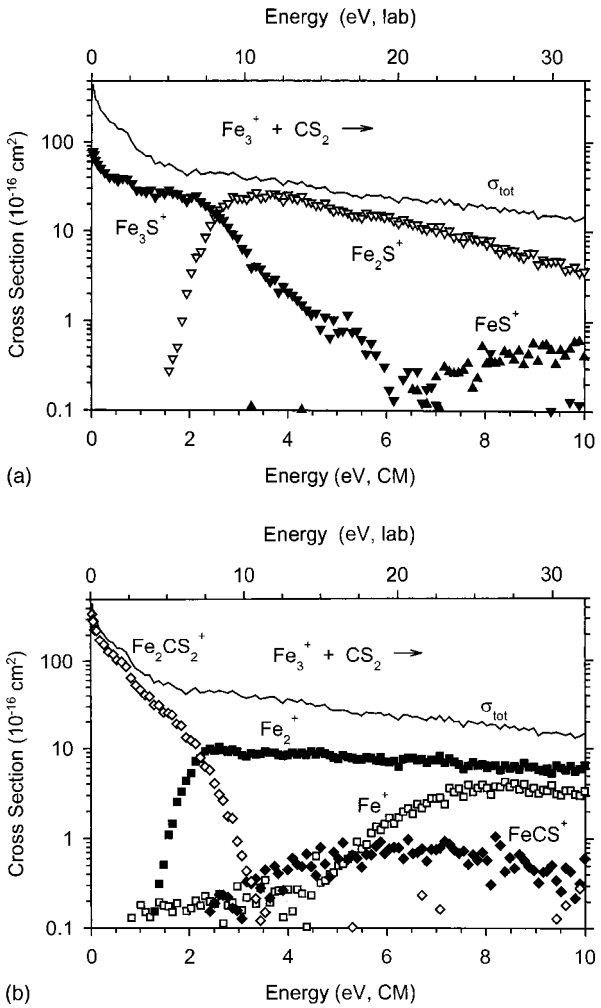

FIG. 5. Main-product cross sections for the reaction of Fe_3^+ with CS_2 as a function of center-of-mass energy (lower axis) and laboratory energy (upper axis). For minor products observed, see text. (a) Sulfur-transfer reactions. (b) Other reactions.

The cross sections of the remaining products, $Fe_2S_2^+$ and the formal adduct $Fe_2CS_2^+$, are both pressure-dependent suggesting their formation via multiple collisions. Although $Fe_2S_2^+$ also was observed in the system Fe_2^+/COS, the equivalent of $Fe_2CS_2^+$ did not occur. Apparently, Fe_2COS^+ has a lowered probability to undergo termolecular stabilization because $D_0(SFe_2^+-CO)<D_0(SFe_2^+-CS)$. Another rationale for this observation might be that some amount of $Fe_2CS_2^+$ is formed with an intact CS_2 ligand whereas the lower C–S bond strength in COS strongly favors facile sulfur-atom-transfer followed by loss of the carbonyl ligand.

The reaction between Fe_3^+ and CS_2 (Fig. 5) yields Fe_3S^+ as the primary product of an exothermic sulfur transfer, reaction (14) with $x=0$,

$$Fe_3^+ + CS_2 \rightarrow Fe_{3-x}S^+ + xFe + CS. \quad (14)$$

At higher energies, the secondary product Fe_2S^+ and then the tertiary product FeS^+ emerge, reaction (14) with $x=1$ and 2, respectively. Although the BDE of a hypothetical product FeCS is not known, in analogy with FeCO (see above), a weak binding between neutral Fe and a CS ligand is expected, such that formation of FeCS is deemed improbable compared to that of separated Fe and CS. The main product at low energies is $Fe_2CS_2^+$, formed in reaction (15a), which has no counterpart in the Fe_3^+/COS system (see above),

$$Fe_3^+ + CS_2 \rightarrow Fe_2CS_2^+ + Fe, \quad (15a)$$

$$Fe_3^+ + CS_2 \rightarrow Fe^+ + Fe_2CS_2. \quad (15b)$$

The initial step of this reaction is suggested to be the insertion of the metal core into the S–CX bond, similar to the first step of the generally assumed sulfur-transfer mechanism.[49,58] Whereas the CX moiety is ejected for both X=O and S, thus effecting sulfur transfer, loss of Fe only occurs for X=S. Apparently, the CS fragment is bound more strongly than Fe, i.e., $D_0(Fe_3S^+-CS)>D_0(Fe_2CS_2^+-Fe)$, such that the loss of the metal atom is preferred. In addition to the formation of $Fe_2CS_2^+$ concomitant with Fe, reaction (15a), the same products can be generated with inverted charge distribution, reaction (15b). This process is assigned as the energetically most favorable pathway to form Fe^+ and thus to account for the low-energy feature in its cross section (below 4 eV). It shows a poor efficiency resulting from the dominance of the competing reaction (15a), thus indicating $IE(Fe_2CS_2)<IE(Fe)=7.90\,eV$.[54] At higher energies, Fe^+ can arise from simple CID of Fe_3^+, starting at about 4.53 ± 0.16 eV and consistent with the main feature in the Fe^+ cross section. Likewise, the threshold of the Fe_2^+ channel agrees with $D_0(Fe_2^+-Fe)=1.75\pm0.12\,eV$ (Table I) and is thus assigned to simple CID of Fe_3^+. In turn, the experiment provides no indication that a hypothetical species $FeCS_2$ having an appreciable BDE rather than separated Fe and CS_2 is formed. Further, $FeCS^+$ is observed as a minor product ($\sigma_{max}<1.0\,Å^2$). Because of its relatively early apparent threshold [$\approx$2 eV, off scale in Fig. 5(b)], the concomitant neutral is more likely to be Fe_2S than FeS and Fe. Thus, $FeCS^+$ is probably a primary reaction product arising from reaction between Fe_3^+ and CS_2 and not from the decomposition of $Fe_2CS_2^+$. Additional products, $Fe_3S_2^+$ and $Fe_3S_3^+$, show pressure-dependent cross sections, which indicate their formation via multiple collisions, and are not pursued any further.

The Fe_4^+/CS_2 and Fe_5^+/CS_2 systems are closely related (illustrated for the latter in Fig. 6). The primary sulfur-transfer channels yielding Fe_nS^+, reaction (16) with $x=0$,

$$Fe_n^+ + CS_2 \rightarrow Fe_{n-x}S^+ + xFe + CS, \quad (16)$$

are exothermic again but display bimodal features at low energies. The successive appearance of the endothermic products $Fe_{n-1}S^+$, $Fe_{n-2}S^+$, and even $Fe_{n-3}S^+$ for $n=5$, reaction (16) with $x=1-3$, suggests that single Fe atoms are lost sequentially, in analogy to the COS systems discussed above. At low energies, the $Fe_{n-1}CS_2^+$ products prevail, reaction (17) with $x=1$. Their formation has already been explained for the analogous case of Fe_3^+/CS_2. Elevated kinetic energies result in consecutive fragmentations yielding $Fe_{n-2}CS_2^+$ and even $Fe_{n-3}CS_2^+$ for $n=5$, reaction (17) with $x=2$ and 3, respectively,

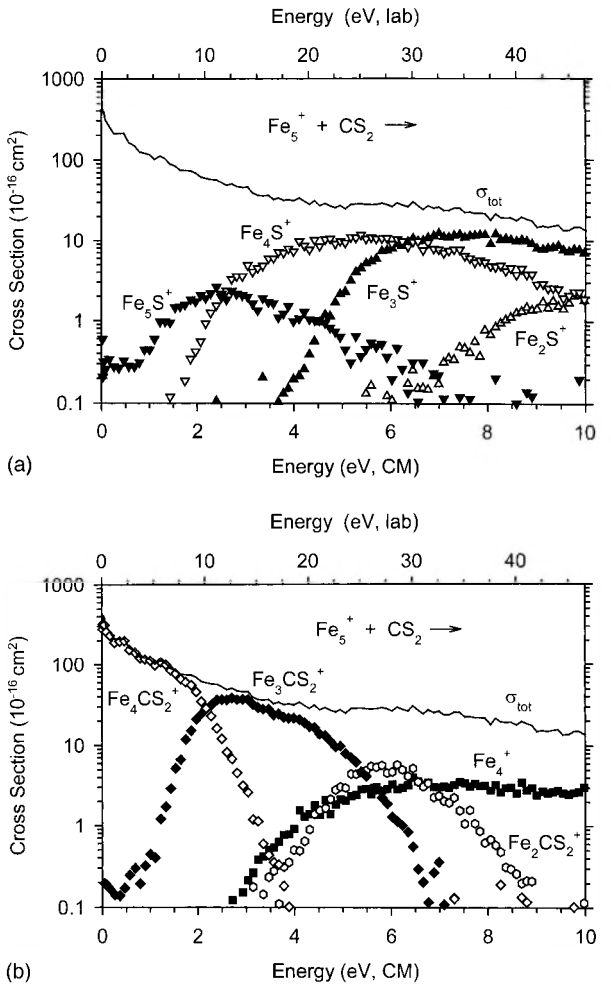

FIG. 6. Main-product cross sections for the reaction of Fe_5^+ with CS_2 as a function of center-of-mass energy (lower axis) and laboratory energy (upper axis). For minor products observed, see text. (a) Sulfur-transfer reactions. (b) Other reactions.

$$Fe_n^+ + CS_2 \rightarrow Fe_{n-x}CS_2^+ + xFe. \quad (17)$$

Additionally, the bare Fe_{n-x}^+ cluster ions ($x=1-3$ for $n=4$ and $x=1$ for $n=5$) observed as products are attributed to simple CID reactions. Further, formation of termolecular products, like $Fe_{n-1}CS_3^+$, takes place to some extent at low energies with pressure dependent cross sections.

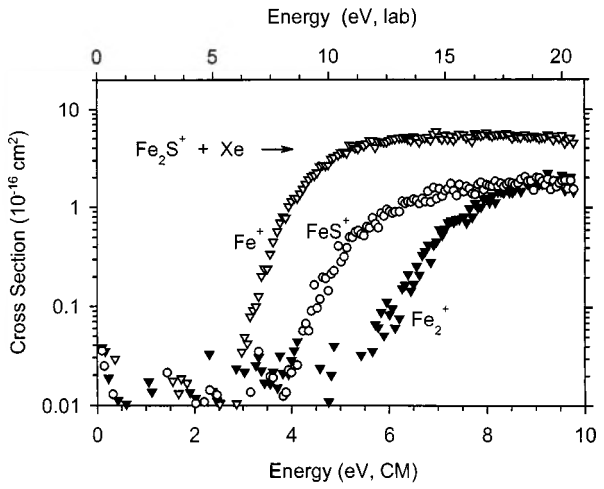

FIG. 7. Product cross sections for the collision-induced dissociation of Fe_2S^+ with Xe as a function of center-of-mass energy (lower axis) and laboratory energy (upper axis).

Despite the manifold of reactions observed in the Fe_n^+/COS and Fe_n^+/CS_2 systems, a qualitative synopsis reveals that the major processes can be assigned to a relatively small number of reaction types (Table II). For Fe_n^+/COS, the primary reactions are almost exclusively sulfur transfers (Ia). For Fe_n^+/CS_2, substitutions of one Fe atom for CS_2 are equally important (Ib). The other products result from successive dissociations of these primary products. The importance of such secondary (II), tertiary (III), and quaternary reactions (IV) has also been reported for other reactions of cationic iron clusters.[24,26,29]

3. Reactions of Fe_nS^+ with Xe

Upon reacting Fe_nS^+ ($n=2-4$) with xenon, no processes other than simple CID are observed. These fragmentations are equivalent to the decomposition processes seen for the primary Fe_nS^+ species formed from Fe_n^+ and CXS at elevated energies (see above).

For Fe_2S^+, the ionic products observed are Fe^+, FeS^+, and Fe_2^+ (Fig. 7). As in the Fe_2^+/CXS system, the neutral concomitantly formed with Fe^+ has to be FeS rather than the separated atoms to account for the early appearance of this

TABLE II. Main products (■) of the reactions between Fe_n^+ and CXS (X=O, S).[a]

		Fe^+[b]		Fe_2^+		Fe_3^+		Fe_4^+		Fe_5^+		Fe_6^+
	Reaction type	COS	CS_2	COS	CS_2	COS	CS_2	COS	CS_2	COS	CS_2	COS
Ia	$Fe_nS^+ + CX$	■	■	■	■	■	■	■	■	■	■	■
Ib	$Fe_{n-1}CXS^+ + Fe$		■				■		■		■	
IIa	$Fe_{n-1}S^+ + Fe + CX$			■	■	■	■	■	■	■	■	■
IIb	$Fe_{n-2}CXS^+ + 2Fe$								■		■	
IIc	$Fe_{n-1}S + Fe^+ + CX$			■	■							
IIIa	$Fe_{n-2}S^+ + 2Fe + CX$					■	■	■	■	■	■	■
IIIb	$Fe_{n-3}CXS^+ + 3Fe$										■	
IVa	$Fe_{n-3}S^+ + 3Fe + CX$									■	■	■

[a]Simple CID products are omitted.
[b]Taken from Ref. 49.

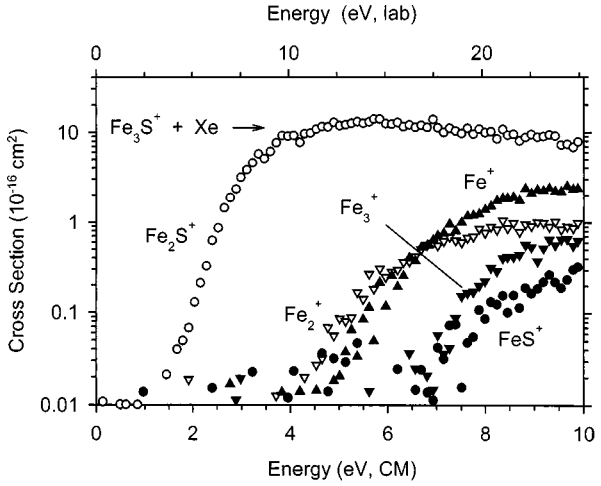

FIG. 8. Product cross sections for the collision-induced dissociation of Fe_3S^+ with Xe as a function of center-of-mass energy (lower axis) and laboratory energy (upper axis).

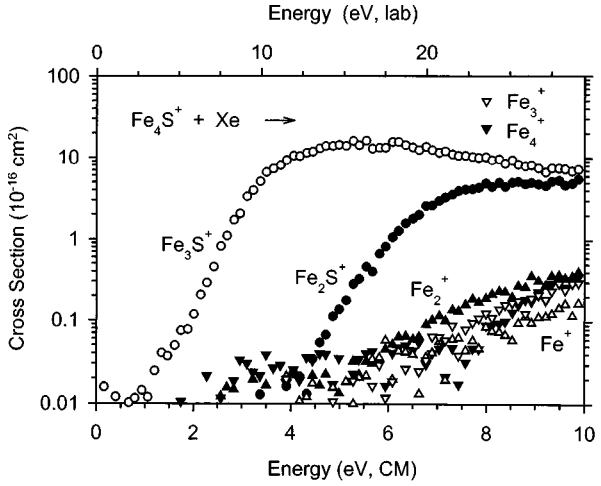

FIG. 9. Main-product cross sections for the collision-induced dissociation of Fe_4S^+ with Xe as a function of center-of-mass energy (lower axis) and laboratory energy (upper axis).

channel, reaction (18a). Again, localization of the positive charge at Fe rather than FeS, formed according to reaction (18b),

$$Fe_2S^+ + Xe \rightarrow Fe^+ + FeS + Xe \quad (18a)$$

$$\rightarrow FeS^+ + Fe + Xe, \quad (18b)$$

is favored in agreement with the difference in the IEs. Because both reactions compete with each other, the energetically more demanding reaction (18b) bears a delayed apparent threshold ($\Delta E_0 \approx 1.0$ eV vs ΔIE$=0.4$ eV). Cleavage of the iron–sulfur bond to yield Fe_2^+ is even more energy-demanding, reaction (19),

$$Fe_2S^+ + Xe \rightarrow Fe_2^+ + S + Xe. \quad (19)$$

For Fe_3S^+, the energetically most favorable CID product is Fe_2S^+ resulting from loss of Fe, reaction (20) (Fig. 8),

$$Fe_3S^+ + Xe \rightarrow Fe_2S^+ + Fe + Xe. \quad (20)$$

In contrast to reactions (18a) and (18b), the analogous process yielding the inverse charge distribution, i.e., $Fe^+ + Fe_2S$, does not seem to be operative, because the Fe^+ channel is shifted to higher energies by more than 3 eV. It is unlikely that the difference in IEs and competition effects could account for this amount. Rather, consecutive fragmentation of the corresponding Fe_2S^+ product, as in reaction (18a), appears to give rise to $Fe^+ + FeS + Fe$. Likewise, FeS^+ is probably formed by decomposition of Fe_2S^+, Fe_3^+ by loss of S from Fe_3S^+, and Fe_2^+ is accompanied by FeS because the apparent threshold is inconsistent with formation by Fe loss from Fe_3^+.

CID of Fe_4S^+ results in the formation of Fe_3S^+ as the single product seen at low energies, reaction (21) with $x = 1$ (Fig. 9),

$$Fe_4S^+ + Xe \rightarrow Fe_{4-x}S^+ + xFe + Xe. \quad (21)$$

Its cross section declines at higher energies as the Fe_2S^+ channel appears. This suggests that the latter arises from consecutive dissociation of the former in reaction (21) with $x = 2$. The Fe_n^+ products ($n = 1-4$), which have small cross sections, are not analyzed any further.

4. Reactions of Fe_nS^+ with CS_2

The reaction between Fe_2S^+ and CS_2 yields $Fe_2S_2^+$ as the main product at lower energies, reaction (22) with $x = 0$ (Fig. 10),

$$Fe_2S^+ + CS_2 \rightarrow Fe_{2-x}S_2^+ + xFe + CS. \quad (22)$$

The cross section decreases with increasing energies, behavior characteristic of an exothermic process, hence $D_0(SFe_2^+-S) > D_0(SC-S) = 4.50 \pm 0.04$ eV. This is in marked contrast to the analogous sulfur transfer from CS_2 onto Fe_2^+, reaction (13), which proved to be endothermic. Hence, the qualitative analysis indicates $D_0(SFe_2^+-S) > D_0(Fe_2^+-S)$. Between 2–4 eV, the $Fe_2S_2^+$ cross section levels out, suggesting the possibility that another, endothermic pathway becomes available. As the primary sulfur-transfer reactions observed in the Fe_n^+/CXS systems showed similar bimodal behaviors, the possible explanation proposed above can also account for the case of $Fe_2S_2^+$. At higher energies, the cross section of $Fe_2S_2^+$ starts to decline again, while that of FeS_2^+ rises. Obviously, the latter results from dissociation of $Fe_2S_2^+$, reaction (22) with $x = 1$.

The endothermic formation of $FeCS^+$ is inefficient ($\sigma_{max} \sim 0.4$ Å^2) and its energy threshold cannot be inferred unambiguously. Additionally, the products Fe^+ and FeS^+ are observed and are mainly attributed to CID as they have similar energy dependences as in the experiments using Xe as collision gas (Fig. 7). However, these products may partly arise from decompositions of $Fe_2S_2^+$ and FeS_2^+, and their cross sections are therefore not used for drawing any thermochemical conclusions. The energy dependences of Fe_2^+ differ notably for Xe and CS_2, indicating that in the reaction with the latter a process other than simple CID is operative. The relatively early appearance of Fe_2^+ could be rationalized by the formation of CS_3 as the neutral product [$D_0(S_2C-S) = 0.22 \pm 0.14$ eV],[9] although the efficiency ob-

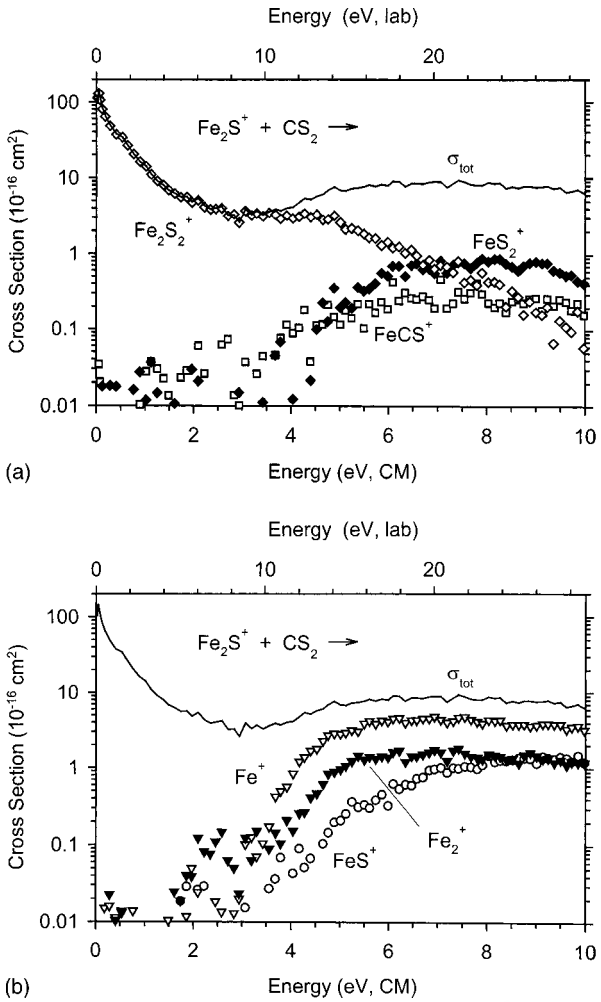

FIG. 10. Main-product cross sections for the reaction of Fe_2S^+ with CS_2 as a function of center-of-mass energy (lower axis) and laboratory energy (upper axis). For minor products observed, see text. (a) Sulfur- and carbon-transfer reactions. (b) CID and other reactions.

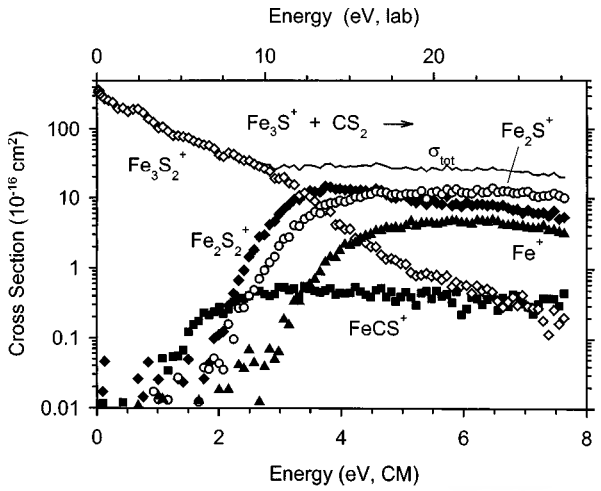

FIG. 11. Main-product cross sections for the reaction of Fe_3S^+ with CS_2 as a function of center-of-mass energy (lower axis) and laboratory energy (upper axis). For minor products observed, see text.

served appears higher than one would expect for this reaction. In contrast, a process accounting for the rather high efficiency of this channel but not for its early threshold would be the formation of S_2 and CS as neutral products, 0.36 eV higher in energy than CS_3. Thus, we conclude that the Fe_2^+ cross section does not reflect a single reaction but rather a mixture of different processes such that an unambiguous assignment is not possible. In addition, multiple collisions result in the formation of $Fe_2CS_3^+$, $Fe_2CS_4^+$, and even $Fe_2C_2S_6^+$ at low energies.

The Fe_3S^+/CS_2 system (Fig. 11) very much resembles its smaller homolog. The primary sulfur transfer to form $Fe_3S_2^+$ is exothermic, whereas subsequent loss of Fe and formation of $Fe_2S_2^+$ occur at higher energies, reaction (23),

$$Fe_3S^+ + CS_2 \rightarrow Fe_2S_2^+ + Fe + CS, \tag{23}$$

$$Fe_3S^+ + CS_2 \rightarrow FeCS^+ + Fe_2S_2. \tag{24}$$

Moreover, $FeCS^+$ as well as Fe_3^+, Fe_2S^+, Fe_2^+, and Fe^+ are formed (the minor products Fe_2^+ and Fe_3^+ are omitted in Fig. 11). For most of these products, the energy dependencies are similar to the CID products observed with xenon (Fig. 8). The $FeCS^+$ fragment is interesting as its energy threshold is relatively low, $E_0 = 1.33$ eV. The reaction clearly involves formation of a Fe^+–CS bond, which releases 2.40 ± 0.12 eV, and cleavage of the SC–S bond ($D_0 = 4.50 \pm 0.04$ eV) and the Fe^+–Fe_2S bond. Formation of $Fe_2S + S$ as neutral products is inconsistent with the low threshold energy observed, indicating that the neutral product is Fe_2S_2, reaction (24). Thus, the reaction can be considered the equivalent of reaction (23) with an inverted charge distribution. Localization of the positive charge on the Fe atom greatly enhances the attraction between the metal and CS such that bond formation occurs, whereas no strong interaction between neutral Fe and CS is expected (see above). In this respect, experiments explicitly probing the stability of neutral FeCS would be particularly helpful. Similarly, the formation of Fe^+ with a threshold ($E_0 = 3.26 \pm 0.11$ eV) about 2 eV lower than in Fig. 8, where the reaction clearly forms $Fe^+ + FeS + Fe$, indicates that the reaction with CS_2 provides more stable neutral products, e.g., $Fe_2S + CS_2$, $Fe_2S_2 + CS$, or even Fe_2CS_3. In addition to the products shown in Fig. 11, we also observe $Fe_3S_3^+$, $Fe_2CS_4^+$, and $Fe_2C_2S_6^+$, which are formed at low energies by multiple collisions and are not discussed any further.

Fe_4S^+ reacts exothermically with CS_2 to give $Fe_4S_2^+$, reaction (25) with $x = 0$ (Fig. 12). At higher energies, $Fe_3S_2^+$ and $Fe_2S_2^+$ appear successively and are attributed to sequential losses of Fe atoms from $Fe_4S_2^+$, reaction (25) with $x = 1$ and 2, respectively,

$$Fe_4S^+ + CS_2 \rightarrow Fe_{4-x}S_2^+ + xFe + CS. \tag{25}$$

The products Fe_4^+, Fe_3S^+, Fe_3^+, Fe_2S^+, Fe_2^+, and Fe^+ (only the major products Fe_3S^+ and Fe_2S^+ are shown in Fig. 12) are attributed to CID. Multiple collisions account for the formation of $Fe_4S_3^+$, $Fe_4CS_3^+$, and $Fe_4S_4^+$ at low energies.

Comparing the Fe_n^+/CS_2 (Table II) and Fe_nS^+/CS_2 (Table III) systems, sulfur-transfer reactions readily take

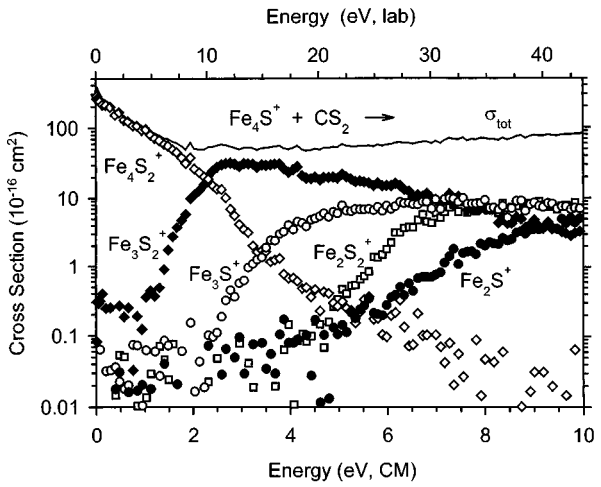

FIG. 12. Main-product cross sections for the reaction of Fe_4S^+ with CS_2 as a function of center-of-mass energy (lower axis) and laboratory energy (upper axis). For minor products observed, see text.

place for both of them. At elevated energies, the primary products having excess energy lose Fe atoms. In contrast to the Fe_n^+/CS_2 system, however, displacement of Fe by CS_2 does not occur in the case of Fe_nS^+/CS_2. A rationale for this difference will be given on the basis of the thermochemistry developed below.

B. Quantitative analysis of cross sections

From the energy threshold of a reaction cross section, the reaction enthalpy of the corresponding process can be extracted. The determination of thermochemically accurate data from GIB experiments requires the absence of any appreciable barriers in excess of the overall endothermicity for the reaction investigated. For sulfur-transfer reactions between CXS (X=O, S) and metal cations, the appropriateness of the GIB approach has already been demonstrated above.[9] However, all primary sulfur-transfer reactions of the bare Fe_n^+ clusters studied (reaction type Ia, Table II), except that between Fe_2^+ and CS_2, reaction (13), are exothermic so that no thresholds can be determined. The same holds true for the primary sulfur-transfer reactions between Fe_nS^+ and CS_2 (Table III). Thus, these reactions only provide lower limits for $D_0(Fe_n^+-S)$ and $D_0(SFe_n^+-S)$. The alternative usage of reagents having stronger bonds to sulfur, e.g., SO_2 [$D_0(O_2-S)=5.90\pm0.01$ eV (Ref. 51)], does not appear feasible either, because the release of S from these compounds requires considerable rearrangements that could lead to significant barriers, and other reactions, e.g., O-transfer, seem to be more likely. Nevertheless, the experiments involving the Fe_n^+/CXS and Fe_nS^+/CS_2 systems can be used for the extraction of Fe–S BDEs by analyzing the secondary reactions (IIa) yielding $Fe_{n-1}S^+$ and $Fe_{n-1}S_2^+$, respectively. A similar procedure has been successfully applied in the determination of Fe_n^+-D, Fe_n^+-C, Fe_n^+-CD bond energies from reactions with [D_4]-methane,[29] where values from both primary and secondary reactions could be compared directly. In the present study, Fe–S BDEs can be derived by applying Born–Haber cycles [Fig. 13, Eqs. (26) and (27)].

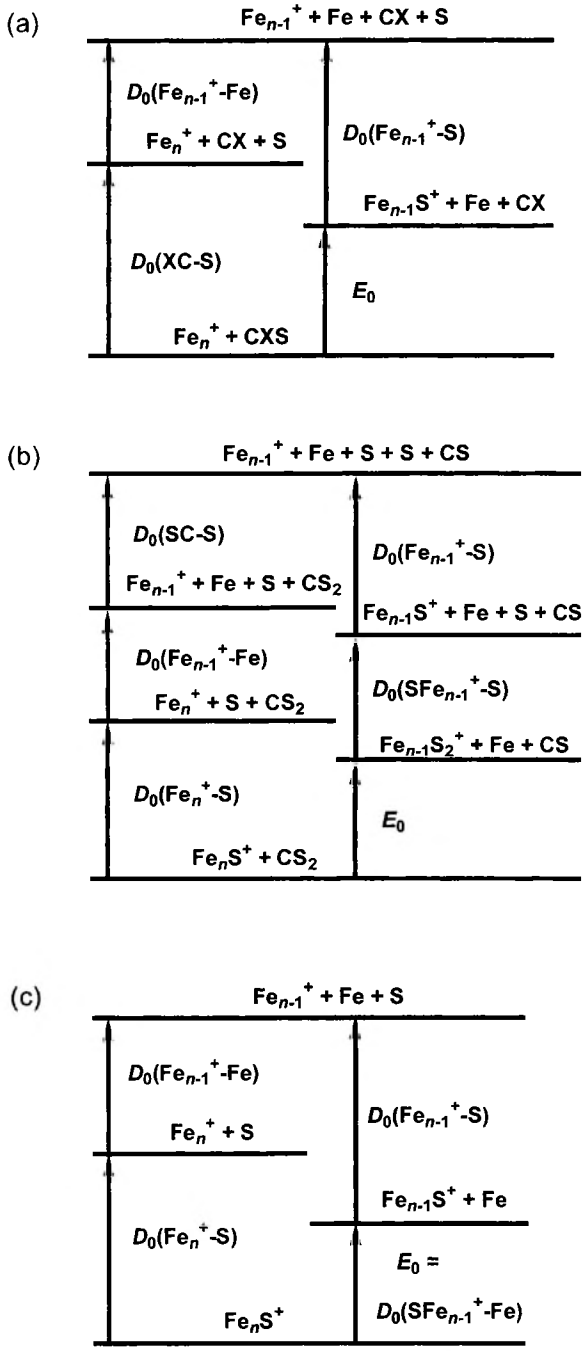

FIG. 13. Born–Haber cycles. (a) Reaction type IIa, $Fe_n^+ + CXS \rightarrow Fe_{n-1}S^+ + Fe + CX$. (b) Reaction type IIa, $Fe_nS^+ + CS_2 \rightarrow Fe_{n-1}S_2^+ + Fe + CS$. (c) Collision-induced dissociation, $Fe_nS^+ + Xe \rightarrow Fe_{n-1}S^+ + Fe + Xe$.

TABLE III. Main products (■) of the reactions between Fe_nS^+ and CS_2.[a]

	Reaction type	FeS^+[b]	Fe_2S^+	Fe_3S^+	Fe_4S^+
Ia	$Fe_nS_2^+ + CS$	■	■	■	■
Id	$Fe_nCS^+ + S_2$	■			
IIa	$Fe_{n-1}S_2^+ + Fe + CS$		■	■	■
IIe	$FeCS^+ + Fe_{n-1}S_2$			■	
IIIa	$Fe_{n-2}S_2^+ + 2Fe + CS$				■

[a]Simple CID products are omitted.
[b]Taken from Ref. 49.

$$D_0(Fe_{n-1}^+-S)=D_0(XC-S)+D_0(Fe_{n-1}^+-Fe)-E_0, \quad (26)$$

$$\begin{aligned} D_0(SFe_{n-1}^+-S)&=D_0(Fe_n^+-S)+D_0(Fe_{n-1}^+-Fe)\\ &\quad +D_0(SC-S)-D_0(Fe_{n-1}^+-S)-E_0\\ &=\Delta_{n-1/n}D_0+D_0(Fe_{n-1}^+-Fe)\\ &\quad +D_0(SC-S)-E_0. \end{aligned} \quad (27)$$

To this end, the consideration of differential BDEs $\Delta_{n-1/n}D_0=D_0(Fe_n^+-S)-D_0(Fe_{n-1}^+-S)$ is particularly helpful. Complementary information is provided by the CID experiments. Given that energy deposition is efficient, the threshold of a CID reaction directly corresponds to the BDE of the bond broken. In the present work, only the lowest energy CID reactions of iron–sulfur clusters Fe_nS^+, i.e., Fe losses, reactions (18), (20), and (21) (with $x=1$), but no S losses, are considered in order to avoid competitive shifts for the higher-lying CID channels. The energy thresholds are related to Fe–S BDEs by another Born–Haber cycle [Fig. 13, Eq. (28)],

$$\begin{aligned} \Delta_{n-1/n}D_0&\equiv D_0(Fe_n^+-S)-D_0(Fe_{n-1}^+-S)\\ &=D_0(SFe_{n-1}^+-Fe)-D_0(Fe_{n-1}^+-Fe)\\ &=E_0-D_0(Fe_{n-1}^+-Fe). \end{aligned} \quad (28)$$

Some modification is necessary in the case of CID of Fe_2S^+, reaction (18a), where the S containing fragment is neutral. Here, the threshold of the Fe^+ cross section (concomitant with neutral FeS) bears information on $D_0(Fe-S)$, implying another thermochemical cycle [Eq. (29)],

$$\begin{aligned} \Delta_{1/2}D_0'&\equiv D_0(Fe_2^+-S)-D_0(Fe-S)\\ &=D_0(SFe^+-Fe)-D_0(Fe^+-Fe)\\ &=E_0-D_0(Fe^+-Fe). \end{aligned} \quad (29)$$

Similarly, $Fe^+ + FeS + CX$ also arises from the secondary reactions observed for Fe_2^+/CXS (IIa). However, the simultaneous occurrence of CID forming $Fe^+ + Fe + CXS$ is probable. Thus, the experimental cross sections presumably reflect both processes, which makes them difficult to analyze unambiguously.

Finally, from reaction (24), the IE of Fe_2S_2 can be derived according to Eq. (30),

$$\begin{aligned} IE(Fe_2S_2)&=IE(Fe)+D_0(SC-S)+D_0(SFe_2^+-Fe)\\ &\quad -D_0(SFe_2^+-S)-D_0(Fe^+-CS)-E_0. \end{aligned} \quad (30)$$

Here, determination of an IE instead of a BDE implies a thermochemical cycle different from those presented above.

As mentioned above, an accurate threshold analysis requires knowledge of the molecular properties of the species involved in the reactions studied. For COS and CS_2, vibrational modes and rotational constants are well-known.[59] For Fe_n^+ and Fe_nS^+ clusters, however, scarce information is available. Therefore, an elastic model proposed by Shvartsburg *et al.* is applied to estimate the vibrational modes of iron clusters Fe_n^+.[60] Basically, this model derives molecular constants from properties of the bulk metal. The method for estimating the rotational constants draws on the metal's crystal structure.[26] For iron–sulfur clusters $Fe_nS_m^+$ ($m=1,2$), molecular constants are obtained by combining those derived for Fe_n^+ with $Fe_\infty-S$ vibrations extracted from surface studies. The RRKM treatment based on Eq. (3) considers both tight and loose transition structure (TS) models as limiting cases and averages the results derived from both approaches. All technical details are given in the Appendix that also addresses the uncertainties associated with the various assumptions.

For the secondary reactions (IIa), the RRKM analysis also has to take into account their multistep mechanisms. Because the initial, exothermic sulfur transfer obviously occurs much more rapidly than the subsequent, endothermic loss of Fe, the RRKM modeling can be restricted to the rate-limiting second step of the reaction, the unimolecular decomposition, which is just identical to the corresponding CID process. However, the reaction enthalpy of the exothermic primary process forming the EM, E_1, does have an indirect effect by raising the effective temperature of the EM and, thus, influencing the decomposition rate. The model employed accounts for this effect by including E_1 in the energy available for the consecutive dissociation step, E^* [Eq. (31)],

$$E^*=E_T-\Delta E-E_1. \quad (31)$$

Yet, the determination of E_1 requires the value of $D_0(Fe_n^+-S)$, which is to be determined in the very same threshold analysis. Obviously, an iterative method has to be applied. For the largest system studied, Fe_6^+/COS, an initial guess of $D_0(Fe_6^+-S)$ is necessary. A comparison with the BDEs of the related iron-oxide clusters shows that $D_0(Fe_6^+-O)\approx D_0(Fe_5^+-O)$.[28] Further, the CID experiments of Fe_nS^+ ($n=2-4$) show that the differential BDEs, $\Delta_{n-1/n}D_0$, diminish monotonically as the cluster size n increases (see below). Hence, it appears reasonable to assume $D_0(Fe_6^+-S)\approx D_0(Fe_5^+-S)\pm 0.5\,eV$ as initial input. Fortunately, the threshold analysis is not particularly sensitive to variations in E_1 because the reaction enthalpy of the primary reaction step E_1 does not affect the threshold directly, but only alters the kinetic shift. Neglecting E_1 in a first step of the threshold analysis provides an initial guess for $D_0(Fe_5^+-S)\approx D_0(Fe_6^+-S)$ which then allows derivation of E_1 as an input parameter for an improved analysis, and so forth. Self-consistency within 0.01 eV is reached after a few cycles. To take into account the error associated with the final assumption for E_1, the analysis is repeated after increasing and decreasing E_1 by 0.5 eV. The uncertainties in the thresholds E_0 introduced by this variation amount to ± 0.09 eV. Moreover, the CID results were also taken into account with respect to the reaction enthalpies of the primary step E_1. Analogous methods are applied for the secondary reactions between Fe_nS^+ and CS_2. Because the raw data suggest $D_0(SFe_n^+-S)\approx D_0(Fe_n^+-S)+0.5\,eV$ for $n=1-3$, the same relationship is assumed for $n=4$. Again, the uncertainty of this guess is estimated at ± 0.5 eV.

When the exothermicity of the first step of secondary reactions is deliberately neglected in the RRKM analysis, the kinetic shifts are significantly reduced in comparison to the proper treatment that includes E_1 (Table IV). This result may

TABLE IV. Dependence of kinetic shifts on the reaction enthalpy of the initial reaction step, E_1, exemplified for Fe_n^+/COS, reaction type IIa. All energies given in eV.

			Kinetic shifts, E_1 neglected		Kinetic shifts, E_1 included	
n	E_0[a]	E_1	LTS	TTS	LTS	TTS
2[b]	1.66	−1.08	0.00	0.00	0.00	0.00
3	0.81	−1.80	0.00	0.00	0.00	0.03
4	0.55	−2.15	0.00	0.02	0.02	0.14
5	0.58	−2.27	0.00	0.04	0.13	0.38
6	1.00	−2.27	0.08	0.25	0.38	0.78

[a]Average of LTS and TTS models with E_1 included.
[b]Not further investigated in the threshold analysis because of the probability of other interfering reactions.

appear surprising because an increase in the internal energy of an intermediate is generally assumed to accelerate its decomposition. To resolve this seeming paradox, note that the energy required for dissociation of the Fe_nS^+ ion in the experiment is not the endothermicity of the overall reaction, E_0, but that of the decomposition step, $E_2 = E_0 - E_1$. Thus, the number of states at the TS has to be evaluated at the energy $E^*_{CID} - E_1 - E_2 = E^*_{CID} - E_0$, such that the rate is given by Eq. (32),

$$k(E^*_{sec}) = k(E^*_{CID} - E_1) = sN^{\ddagger}(E^*_{CID} - E_0)/\rho(E^*_{CID} - E_1), \tag{32}$$

where E^*_{sec} and E^*_{CID} are the energy contents of the EM for secondary and CID reactions, respectively, which differ by E_1. Obviously, decreasing E_1 (i.e., making it more negative) reduces the rate constant because it only raises ρ while not affecting $N^{\ddagger}$. In other words, because of the coupling between E_1 and E_2, a decrease in E_1 enlarges the internal energy of the EM but simultaneously deepens its potential well. The latter effect is rate-decelerating and predominates.

Another important feature in the analysis of secondary reactions is that energy can be lost from the initial transient complex as kinetic energy motion of the primary products and as rotational and vibrational excitation of CX. The latter possibility is less probable because of the high frequency of the CX vibrational modes. Nevertheless, the thermodynamic threshold of the secondary process corresponds to the energetically least demanding way to form products (i.e., without any prior loss of energy) and thus to the very onset of the cross section observed, which the modeling procedure is designed to find. The validity of the approach chosen can be tested by comparing the results derived from the experiments using COS and CS_2, respectively. Because of the difference in BDEs, $D_0(SC-S) - D_0(OC-S) = 1.36 \pm 0.04$ eV (Table I), the initial collision complexes, $XC-Fe_nS^+$, clearly contain different amounts of energy for X=O and S, respectively. If energy were lost nonstatistically from these complexes, they should lead to different energetics. Yet, the BDEs derived from the experiments with COS and CS_2 are essentially identical (Table V), which verifies the ability to determine the true thermodynamic onsets in the threshold analyses for these systems.

Similarly, the validity of the other assumptions associated with the threshold analysis can be checked by the internal consistency of the thermodynamic results, which are obtained from several different reactions involving a specific iron–sulfur cluster as reactant (CID) or product [secondary sulfur-transfer reactions (IIa)]. As the molecular parameters used in the RRKM analysis are equivalent for both reaction types, uniform variations in these estimations cause contrary effects in the results. For instance, as the TSs for cleavage of the $SFe_{n-1}-Fe^+$ bonds are made tighter, the kinetic shifts increase, which corresponds to lower thermochemical thresholds E_0 after deconvolution. Hence, although the reaction enthalpy is decreased for both secondary reactions and CID processes, this implies an increased stability of the Fe_nS^+ cluster involved in the case of the former (Fe_nS^+ as product) but a decreased stability in the case of the latter process (Fe_nS^+ as reactant). Thus, erroneous assumptions in the

TABLE V. Summarized results of threshold analyses.

	Reaction	σ_0[a]	N[a]	E_0[a]	$\Delta_{tot}D_0$[b]	Derived quantity in eV
IIa	$Fe_3^+ + COS \rightarrow Fe_2S^+ + Fe + CO$	17±6	1.2±0.3	0.81±0.06	0.12	$D_0(Fe_2^+-S) = 4.08 \pm 0.13$
	$Fe_4^+ + COS \rightarrow Fe_3S^+ + Fe + CO$	52±17	1.0±0.4	0.55±0.10	0.20	$D_0(Fe_3^+-S) = 4.82 \pm 0.22$
	$Fe_5^+ + COS \rightarrow Fe_4S^+ + Fe + CO$	35±12	0.6±0.3	0.58±0.17	0.23	$D_0(Fe_4^+-S) = 5.26 \pm 0.29$
	$Fe_6^+ + COS \rightarrow Fe_5S^+ + Fe + CO$	11±3	1.6±0.3	1.00±0.26	0.25	$D_0(Fe_5^+-S) = 5.41 \pm 0.39$
Ia	$Fe_2^+ + CS_2 \rightarrow Fe_2S^+ + CS$	23±8	0.9±0.3	0.24±0.06	0.04	$D_0(Fe_2^+-S) = 4.27 \pm 0.06$
IIa	$Fe_3^+ + CS_2 \rightarrow Fe_2S^+ + Fe + CS$	81±27	1.2±0.3	2.19±0.11	0.13	$D_0(Fe_2^+-S) = 4.06 \pm 0.17$
	$Fe_4^+ + CS_2 \rightarrow Fe_3S^+ + Fe + CS$	50±17	0.8±0.4	2.00±0.14	0.21	$D_0(Fe_3^+-S) = 4.73 \pm 0.25$
	$Fe_5^+ + CS_2 \rightarrow Fe_4S^+ + Fe + CS$	16±5	1.3±0.3	2.03±0.20	0.24	$D_0(Fe_4^+-S) = 5.17 \pm 0.31$
CID	$Fe_2S^+ + Xe \rightarrow FeS + Fe^+ + Xe$	10±3	1.3±0.2	3.63±0.10	0.10	$D_0(Fe-S) = 3.37 \pm 0.15$[c]
	$Fe_3S^+ + Xe \rightarrow Fe_2S^+ + Fe + Xe$	25±8	1.2±0.4	2.63±0.11	0.12	$D_0(Fe_3^+-S) = 5.10 \pm 0.17$[d]
	$Fe_4S^+ + Xe \rightarrow Fe_3S^+ + Fe + Xe$	24±8	1.4±0.2	2.71±0.14	0.20	$D_0(Fe_4^+-S) = 5.42 \pm 0.27$[d]
IIa	$Fe_2S^+ + CS_2 \rightarrow FeS_2^+ + Fe + CS$	2±0.7	1.1±0.4	4.63±0.16	0.11	$D_0(SFe^+-S) - \Delta_{1/2}D_0 = 2.65 \pm 0.19$
	$Fe_3S^+ + CS_2 \rightarrow Fe_2S_2^+ + Fe + CS$	42±14	1.4±0.4	2.47±0.15	0.13	$D_0(SFe_2^+-S) - \Delta_{2/3}D_0 = 3.78 \pm 0.20$
	$Fe_4S^+ + CS_2 \rightarrow Fe_3S_2^+ + Fe + CS$	74±25	1.6±0.2	1.55±0.18	0.21	$D_0(SFe_3^+-S) - \Delta_{3/4}D_0 = 5.18 \pm 0.28$
IIe	$Fe_3S^+ + CS_2 \rightarrow FeCS^+ + Fe_2S_2$	0.7±0.2	1.2±0.2	1.33±0.18	0.12	$IE(Fe_2S_2) = 6.64 \pm 0.37$

[a]Fitting parameters according to Eq. (2), σ_0 in 10^{-16} cm^2 eV^{N-1} and E_0 in eV. E_0 is the average of the E_0 values derived from the LTS and TTS model.
[b]Total uncertainty associated with the BDEs of the corresponding Born–Haber cycle, in eV.
[c]Determined on the basis of $D_0(Fe_2^+-S)$ according to Eq. (29).
[d]Determined on the basis of $D_0(Fe_{n-1}^+-S)$ according to Eq. (28).

RRKM analysis would most likely lead to inconsistent thermochemical results.

The values derived for $D_0(Fe_n^+-S)$ agree within their error bars for each cluster size (Table V) where the uncertainties also include statistical errors, the uncertainty in the zero of the energy scale, and the uncertainties introduced by literature values used in Born–Haber cycles, $\Delta_{lit}D_0$ (with geometric addition of uncertainties). The final results are obtained from averaging the various values weighted by their uncertainties (Table VI). These values are then required for determining $D_0(SFe_n^+-S)$ on the basis of the results for the Fe_nS^+/CS_2 systems, where the uncertainties are derived analogously.

V. DISCUSSION

A. Fe_nS^+ clusters

The final results of the $Fe_nS_m^+$ thermochemistry (Table VI) allow evaluations of the chemistry and the associated structural and electronic implications. The BDEs of the monoligated Fe_nS^+ clusters, $D_0(Fe_n^+-S)$, rise monotonically as the cluster size increases and appear to level off at $n\geqslant 4$. The BDEs span a range of more than 2 eV, revealing substantial effects of cluster size. It seems reasonable that the observed increase in bond strength reflects the adoption of multifold coordination. Sulfur is well-known to occupy maximum coordination sites on crystal surfaces of transition metals,[61,62] and multifold bridging is a characteristic feature of molecular iron–sulfur clusters in chemistry and biology.[1,2,63] The large differential BDEs $\Delta_{1/2}D_0=1.14$ eV and $\Delta_{2/3}D_0=0.72$ eV suggest a μ_n-binding of sulfur, i.e., twofold bridging in Fe_2S^+ and threefold bridging in Fe_3S^+. The next step, $\Delta_{3/4}D_0=0.35$ eV, is less pronounced so that it cannot be unambiguously assigned to a further increase in the coordination number of sulfur, i.e., μ_3 versus μ_4 (Scheme 1).

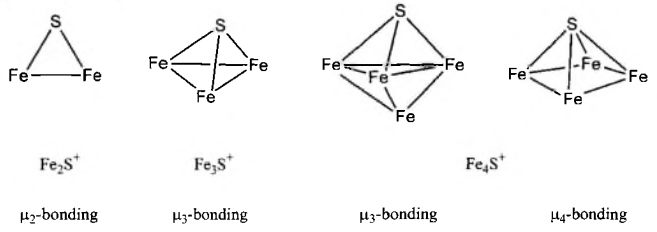

It is not expected that threefold and fourfold coordination sites strongly differ in their energetics. Whereas the interaction between S and the additional fourth Fe atom is assumed to be attractive, the higher steric demands of the fourfold coordination are likely to weaken the individual bondings so that the overall BDE should not be much affected.

The comparison of $D_0(SFe_{n-1}^+-Fe)$ and $D_0(Fe_{n-1}^+-Fe)$ is particularly intriguing because it displays the stabilizing effect of the sulfur atom on the cluster's iron core (Tables I and VI). For all clusters investigated ($n=2-5$), this stabilization is positive with a maximum for $n=2$ and decreasing for the larger clusters. This trend lends further support to the assumed bridging coordination of sulfur. In Fe_2S^+, the interaction between Fe and S is limited necessarily to the two Fe atoms, whereas three or more Fe atoms can contribute in the larger clusters. Therefore, the stabilization the Fe core experiences by ligation of the sulfur ligand, $D_0(SFe_{n-1}^+-Fe) - D_0(Fe_{n-1}^+-Fe)$, is reduced as the cluster size increases, as reflected in the experimental results.

For the smallest cluster studied, Fe_2S^+, computational data are also available (Table VI).[13] Theory predicts slightly lower values for $D_0(Fe_2^+-S)$ and $D_0(SFe^+-Fe)$ than those derived experimentally in this work, but agrees in the relative order, $D_0(Fe_2^+-S)>D_0(SFe^+-Fe)$.

With respect to the function of sulfur as a bridging ligand, it is interesting to compare the present results with other studies of ligated iron clusters (Fig. 14). For small-sized Fe_nD^+ clusters ($n=2-5$), $D_0(Fe_n^+-D)\approx 2$ eV but vary in a manner sensitive to the electronic characteristics of the clusters.[26] Similarly, the bonds formed between Fe_n^+ and the $[D_2]$–methylene fragment do not exhibit a monotonic trend for small cluster sizes, even though the average $D_0(Fe_n^+-CD_2)\approx 3.5$ eV is significantly higher than $D_0(Fe_n^+-D)$.[29] Although the CD_2 fragment may be considered isolobal with a S atom, it obviously adopts a different binding mode when coordinating to Fe_n^+ clusters. Oxygen, however, appears to bind to Fe_n^+ clusters in a manner very similar to that of sulfur.[28,64] The preference of oxygen and sulfur to occupy multifold coordination sites can be rationalized by the availability of electron lone pairs, whereas the CD_2 fragment can at best support μ_2-binding.

B. $Fe_nS_2^+$ clusters

With respect to the thermochemistry of the bis-ligated iron–sulfur clusters, $Fe_nS_2^+$, $n=1-3$, $D_0(SFe^+-S)=3.59\pm 0.12$ eV has previously been extracted from the reaction between FeS^+ and CS_2.[9] From the secondary reaction (IIa) of Fe_2S^+ with CS_2 observed in the present work, one obtains $D_0(SFe^+-S)=3.79\pm 0.21$ eV which is somewhat higher but agrees with the former value within the uncertainties. Further, the photodissociation threshold $[D_{298}(SFe^+-S)=3.82\pm 0.35$ eV] (Ref. 11) of FeS_2^+ converts to $D_0(SFe^+-S)=3.85\pm 0.35$ eV.[9] All these values are significantly larger than the BDE of the monoligated species, $D_0(Fe^+-S)=3.08\pm 0.04$ eV.[9] Analogously, for the clusters $Fe_nS_2^+/Fe_nS^+$, $n=2$ and 3, the binding of the second S atom is enhanced compared to that of the first one (Table VI); however, this need not imply that there are similar bonding modes in these systems. For example, theory predicts that the electronic ground state of FeS_2^+ has a cyclic structure with a disulfide unit.[9] Thereby, the system avoids the unfavorable Fe^V oxidation state that would result from the coordination of two separate sulfido ligands. For $Fe_2S_2^+$ and $Fe_3S_2^+$, however, two sulfido ligands can bind to the cluster core without increasing the metal's average oxidation state anomalously. Indeed, bicapped structures are well-known for various ligated clusters having a Fe_nS_2 core.[1,2,63] In the case of $Fe_2S_2^+$, a rhombic structure has accordingly been predicted by theory[13] and is also inferred from photodissociation experiments.[15] This geometry does not automatically explain the strong binding of the second S atom in $Fe_2S_2^+$ because the first ligand normally causes at least a partial charge and/or valence saturation that reduces the system's affinity

TABLE VI. Bond-dissociation energies of iron–sulfur clusters.[a]

Bond	D_0/eV	Bond	D_0/eV
Fe–S	3.37±0.15		
	3.31±0.15[b]		
Fe^+–S	3.08±0.04[c]	SFe^+–Fe	3.92±0.12[d]
			3.67[e]
Fe_2^+–S	4.22±0.05	SFe_2^+–Fe	2.47±0.18
	4.12[e]		
Fe_3^+–S	4.94±0.12	SFe_3^+–Fe	2.58±0.29
Fe_4^+–S	5.29±0.17	SFe_4^+–Fe	2.82±0.49
Fe_5^+–S	5.41±0.39		
SFe^+–S	3.79±0.20	S_2Fe^+–Fe	4.63±0.33
	3.59±0.12[c]		4.09[e]
	3.85±0.35[f]		
SFe_2^+–S	4.50±0.24	$S_2Fe_2^+$–Fe	3.50±0.46
	3.97[e]		
SFe_3^+–S	5.53±0.35		

[a]This work, unless noted otherwise.
[b]Reference 53.
[c]Reference 9.
[d]Calculated from $D_0(Fe^+–S)$, taken from Ref. 9, and $D_0(Fe_2^+–S)$ according to Eq. (28).
[e]Theoretical results taken from Ref. 13.
[f]Reference 11. Thermal correction according to Ref. 9.

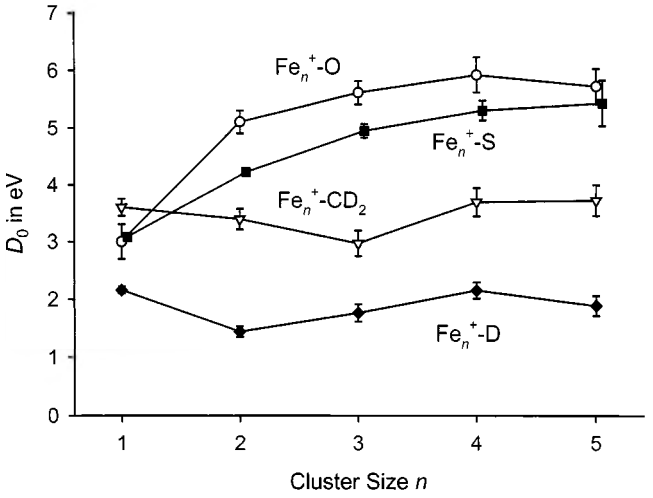

FIG. 14. Bond-dissociation energies $D_0(Fe_n^+–D)$ (Ref. 26), $D_0(Fe_n^+–CD_2)$ (Ref. 29), $D_0(Fe_n^+–O)$ (Refs. 28,64), and $D_0(Fe_n^+–S)$ as function of cluster size. $D_0(Fe^+–S)$ is taken from Ref. 9.

for a further ligand. Ultimately, quantum chemical calculations shall elucidate the character of this system, but a simplified qualitative explanation may be proposed here. In Fe_2^+, the binding is presumed to arise mainly from a $4s$–$4s$ interaction.[30] The addition of a sulfur atom implies an oxidation and, thus, the transfer of electron density from the Fe atoms to S. To achieve a sufficient long-range interaction, the electrons forming the Fe–S bonds should have an appreciable $4s$ character. As a consequence, the Fe–Fe bond is weakened. A favorable binding geometry presumably demands some $3d4s$ mixing, which will cost a certain amount of promotion energy that reduces the overall binding energy. The key to understanding is that both $3d$ and $4s$ orbitals have even symmetry, such that the hybrid orbitals interacting with the S atom on one side of the Fe–Fe axis have the same spatial orientation on the other side. They are therefore ideally suited to form a bond to a second S ligand, resulting in the rhombic $Fe_2S_2^+$. Because the formation of this second bond does not require substantial weakening of the Fe–Fe bond or rehybridization, binding of the second S atom is assumed to be more favorable than that of the first one. This is reflected in the measured order of BDEs, namely, $D_0(Fe_2^+–S) < D_0(SFe_2^+–S)$. Support to the suggested model comes from theory, which predicts a significant lengthening of the Fe–Fe bond from 2.3 to 2.6 Å for the addition of the first S atom to Fe_2^+, but no appreciable further elongation for the addition of the second S ligand.[13] Nevertheless, theory predicts $D_0(Fe_2^+–S) > D_0(SFe_2^+–S)$ by 0.15 eV, in contrast to experiment which finds $D_0(SFe_2^+–S)$ to exceed $D_0(Fe_2^+–S)$ by 0.28 eV (Table VI).

The corresponding $D_0(S_2Fe_n^+–Fe)$ values provide further insight in the stability and structures of small iron–sulfur clusters. The second S ligand causes an appreciable additional stabilization of the Fe atoms in the cluster, consistent with rhombic or bicapped structures, respectively. In $Fe_2S_2^+$, $D_0(S_2Fe^+–Fe)$ is found to slightly exceed $D_0(SFe_2^+–S)$, although the uncertainties associated with these BDEs weaken the reliability of this assignment. For $Fe_3S_2^+$, however, the loss of Fe is unambiguously favored energetically compared to the loss of S, which implies an enhanced stability of $Fe_2S_2^+$. These qualitative conclusions are confirmed by photodissociation experiments of Yu *et al.*:[15] Under UV laser irradiation, loss of S was observed from $Fe_2S_2^+$, whereas Fe was lost from $Fe_3S_2^+$. The stabilizing effect of the S atoms also explains the difference in the reactivities observed in the Fe_n^+/CS_2 and Fe_nS^+/CS_2 systems. In the former, the formal substitution of Fe by CS_2 takes place as an efficient reaction (reaction type Ib), whereas the enhanced stability of the cluster's core prevents the equivalent process in the latter system.

The calculations agree with the experimental findings in predicting a stabilization of the cluster core in $Fe_2S_2^+$ resulting from the ligation of the second S atom, i.e., $D_0(S_2Fe^+–Fe) > D_0(SFe^+–S)$ (Table VI).[13] Also, the relation $D_0(S_2Fe^+–Fe) > D_0(SFe_2^+–S)$ is correctly reproduced by theory. However, the absolute value calculated for $D_0(S_2Fe^+–Fe)$ substantially underestimates the experimental result, as noted above for $D_0(SFe_2^+–S)$. These deviations suggest that the level of theory used in the calculations may not accurately describe the electronic structure of $Fe_2S_2^+$.

C. Neutral Fe_nS_m clusters

Finally, the present work sheds some light on the redox chemistry of $Fe_nS_m^+$ clusters. The IE of FeS exceeds that of Fe,[8] which means that $D_0(Fe–S) > D_0(Fe^+–S)$. Accordingly, the result derived in this work, $D_0(Fe–S) = 3.37 \pm 0.15$ eV, and the value reported in the literature, $D_0(Fe–S) = 3.31 \pm 0.15$ eV,[53] are both larger than $D_0(Fe^+–S) = 3.08 \pm 0.04$ eV.[9] The weaker bonding in the cationic species reflects the electron deficiency at the metal atom, which no longer can provide as much electron density to the electronegative sulfur as the neutral atom. This situation changes when the cluster size increases and the positive

charge is delocalized over the iron core. Although the experiments performed do not quantify the IEs of the Fe_nS clusters, $n=2-5$, the ready losses of neutral Fe atoms from these species (reaction type IIa) indicate that $IE(Fe_nS)<IE(Fe)=7.90\,eV$.[54] Similarly, the high efficiencies of the reactions IIa in the case of the ligated clusters Fe_nS^+ also suggest that $IE(Fe_nS_2)<IE(Fe)$. This hypothesis is further corroborated in the case of Fe_2S_2 for which $IE(Fe_2S_2)=6.64\pm0.35\,eV$ is derived here. The experimental value deviates substantially from the estimate $IE(Fe_2S_2)=7.9\pm0.5\,eV$ given by Hübner *et al.* on the basis of computational results.[14] To understand the origin of this disagreement, a comparison between the stabilities of both the neutral and cationic cluster as derived from experiment and theory is helpful. Using atomization energies as a quantitative measure for the clusters' stabilities, we find that the experimental value for the neutral cluster, $\Delta_{atom}H^{exp}(Fe_2S_2)=10.2\pm0.5\,eV$, is somewhat lower than but within experimental error of the one obtained by theory, $\Delta_{atom}H^{theo}(Fe_2S_2)=10.6\,eV$.[13] On the other hand, for the positively charged cluster, experiment finds a significantly larger stability, $\Delta_{atom}H^{exp}(Fe_2S_2^+\rightarrow Fe^+ + Fe + 2S)=11.5\pm0.3\,eV$, than predicted by theory, $\Delta_{atom}H^{theo}(Fe_2S_2^+)=10.6\,eV$.[13] Hence, the discrepancy between experimental and theoretical results for $IE(Fe_2S_2)$ seems to arise mainly from differences in stability of the cationic cluster.

Compared with $IE(FeS)=8.3\pm0.3$ eV,[8] the experimentally determined value $IE(Fe_2S_2)=6.64\pm0.35\,eV$ lies significantly lower, which can be attributed to enhanced charge delocalization in the larger system. A similar difference is observed for bare iron monomer, $IE(Fe)=7.90\pm0.00$ eV,[54] and dimer, $IE(Fe_2)=6.30\pm0.01\,eV$.[65] On the other hand, the IE of the analogous iron oxide, $IE(Fe_2O_2)=8.4\pm0.3\,eV$, is much larger, which points to differences between the ligand characteristics of sulfur and the more electronegative oxygen.[66] The softer redox properties of the sulfur ligand compared to oxygen have been noted previously in gas-phase iron chemistry.[8]

VI. CONCLUSIONS

The reactions of cationic iron clusters Fe_n^+ with COS ($n=2-6$) and CS_2 ($n=2-5$) are studied in a guided-ion beam mass spectrometer. For both systems, generally exothermic sulfur-transfer reactions readily occur at low energies, and subsequent losses of single Fe atoms prevail at elevated energies. Collision-induced dissociations of independently generated binary clusters Fe_nS^+ ($n=2-4$) fully confirm these results. Similarly, the reactions of Fe_nS^+ with CS_2 bring about sulfur transfer. From modeling of the energy dependences of the various reactions, bond dissociation energies are derived. For the larger clusters studied, the thermochemical analysis requires the consideration of lifetime effects that is achieved by the implementation of RRKM theory. Even though the parameters relevant for the RRKM analysis are not known and have to be estimated, the results derived from the different reactions investigated show good agreement with each other and thus confirm the basic assumptions.

The thermochemical results extracted from the experiments suggest that sulfur occupies multifold coordination sites in the clusters Fe_nS^+ ($n=2-5$) and $Fe_nS_2^+$ ($n=2$ and 3). Such structures resemble those of iron-sulfur clusters in the bulk phase, thus indicating that Fe_nS^+ and $Fe_nS_2^+$ can be used as gas-phase models for the bulk. Among the results obtained, the thermochemical data of $Fe_2S_2^+$ are of particular interest because this species mimics the core of the smallest ferredoxin. The successive bond dissociation energies determined for $Fe_2S_2^+$ reflect its high stability. From this finding one could speculatively infer that the intrinsic stability of the Fe_2S_2 entity forms one contribution to the outstanding role of iron-sulfur clusters in the evolution of life.

ACKNOWLEDGMENTS

Financial support by the Deutsche Forschungsgemeinschaft, the Fonds der Chemischen Industrie, and the Chemical Sciences, Geosciences, and Biosciences Division, Office of Basic Energy Sciences, Office of Science, U.S. Department of Energy is gratefully acknowledged. K.K. thanks the Stiftung Stipendien-Fonds des Verbandes der Chemischen Industrie for a Kekulé scholarship and is grateful to Dr. R. Berger, Dr. O. Hübner, and Dr. I. Kretzschmar for enlightening discussions.

APPENDIX A: TRANSITION STATE MODELS

The RRKM treatment requires assumptions concerning the nature of the energized molecule (EM) and the transition structure (TS) of the reactions considered. For the CID processes to be analyzed, the loss of Fe from Fe_nS^+ (or the loss of Fe^+ concomitant with FeS for $n=2$), the EM is simply the reactant ion. In the TS, the bond connecting the leaving Fe atom and the remaining cluster fragment, $Fe_{n-1}S^+$, is supposed to be partially broken. As already stated above, the same assignments hold for the secondary reactions (IIa), and the corresponding structures in the reactions starting from the ligated clusters Fe_nS^+ only differ by the attachment of a second S atom. For reaction (24) (reaction type IIe), structures analogous to those assigned to reaction (IIa), $n=3$, are assumed. The primary sulfur transfer (Ia) is endothermic only for the reaction of the smallest cluster, Fe_2^+, with CS_2, reaction (13), as outlined above. For such small cluster sizes, lifetime effects are negligible (Table IV) and therefore need not be included in the threshold analysis.

Although the EMs are fully characterized by the molecular constants estimated for Fe_nS^+ (reaction type IIa and CID) and $Fe_nS_2^+$ (reaction type IIa), the corresponding TSs remain to be specified. Without quantum chemical calculations, a localization of the TS on the reaction coordinate is not feasible. Instead, two borderline cases can be distinguished qualitatively. First, the TS is assumed to resemble the EM. If all vibrational modes of the TS equal those of the EM minus the reaction coordinate, a tight TS (TTS) results.[47] Here, the steric restrictions imposed in the transition structure are rather rigid and, thus, only permit a relatively slow decomposition. This corresponds to a large kinetic shift and, after deconvolution, a lower limit for the derived thresholds. The reaction coordinate itself is supposed to correlate with a longitudinal metal–metal vibration of the EM. Because no ad-

TABLE VII. Rotational constants B and vibrational modes ν for Fe_n^+ (all values in cm^{-1}).

n	B	ν_L[a]	$\nu_{T,1}$[b]	$\nu_{T,2}$[b]
2	0.15	300		
3	0.026	232	160	187
4	0.016	163	140	140
		203		174
		234		
5	0.011	148	127	127
		185	158	158
		213		183
		237		
6	0.0083	138	118	118
		171	147	147
		198	170	170
		220		189
		239		

[a]Longitudinal branch.
[b]Transverse branches.

TABLE VIII. Rotational constants B and vibrational modes ν for Fe_nS^+ (all values in cm^{-1}).

n	B	ν_L[a]	$\nu_{T,1}$[b]	$\nu_{T,2}$[b]
1	0.20	463		
		550[c]		
2	0.11	489	394	239
3	0.020	163	270	140
		234		270
		300		
4	0.013	148	158	127
		213	270	183
		237		270
		300		
5	0.0094	138	118	118
		171	170	147
		220	270	189
		239		270
		300		
6	0.0071	130	111	111
		161	138	160
		186	178	178
		225	270	193
		241		270
		300		

[a]Longitudinal branch.
[b]Transverse branches.
[c]Vibrational mode for neutral FeS.

ditional criteria for its selection exist, the medium frequency of the longitudinal branch is chosen as the reaction coordinate. The other extreme is a loose TS (LTS), which assumes a product-like transition structure. Compared to a TTS, a LTS possesses a higher number of rovibrational states, this causing a more rapid dissociation. Therefore, the kinetic shift is smaller and the extracted threshold can be regarded as an upper limit. In this work, the LTS is assumed to be located at the centrifugal barrier, corresponding to a loose association of the products. The transitional modes are treated as rotors, which constitutes a phase space limit.[47] The molecular constants of the LTS are equal to those determined for $Fe_{n-1}S^+$ (IIa and CID) and $Fe_{n-1}S_2^+$ (IIa), respectively. Additionally, the polarizability of the neutral fragment α must be known for specifying its ion-induced dipole-type interaction with the ionic fragment at the centrifugal barrier, $V_{\mathrm{pol}} = -\alpha e^2/8\pi\epsilon_0 r^4$, where e is the elementary charge, ϵ_0 is the permittivity of vacuum, and r is the distance between the ionic and the neutral fragment.[47]

A realistic TS should lie between these two extremes. Accordingly, the arithmetic average of E_0(LTS) and E_0(TTS) is considered a reasonable estimate of the energy threshold at 0 K. Conservatively, the whole difference E_0(TTS) − E_0(LTS) is assigned as the uncertainty associated with the choice of the TS. As the cluster size increases, the kinetic shift and also the deviation between E_0(LTS) and E_0(TTS) grows. For $n=2$, the kinetic shift is <0.01 eV for both TSs and, thus, entirely negligible, whereas for Fe_6^+, the largest cluster studied, the difference E_0(TTS) − E_0(LTS) increases to 0.40 eV (Table IV).

In order to probe the sensitivity of the threshold with respect to the frequency estimations, the threshold analysis was repeated in every case after scaling the entire set of frequencies by factors of 0.5 and 2 for both the LTS and the TTS model. For all reactions analyzed, the resulting deviations are approximately symmetric with respect to the threshold for the unscaled frequencies and are ≤0.06 eV, an exception being the secondary sulfur transfer to Fe_6^+ (IIa) where they amount to 0.08 eV. Hence, the threshold analysis appears not to be particularly sensitive to variations of the molecular constants as a whole.

APPENDIX B: MOLECULAR PARAMETERS OF BARE IRON CLUSTERS Fe_n^+

The vibrational modes for the Fe_n^+ clusters, $n=3-6$ (Table VII), are estimated according to the elastic model suggested by Shvartsburg *et al.*[60] A characteristic of this approach is the formal assignment of the vibrational modes to one longitudinal and two transverse branches. The following quantities of bulk Fe are required as input: the Debye frequency, $\nu_D(\infty)=292\,cm^{-1}$,[67] the ratio of phonon velocities in longitudinal and transverse direction, $c_L/c_T=1.822$ as calculated from elastic constants determined at 4.2 K (arithmetic average of the Hashin and Shtrikman model),[68] and the cutoff frequency for the longitudinal branch of the phonon spectrum, $\nu_{L,\max}=305\,cm^{-1}$ as derived from graphical analysis of the phonon spectrum obtained by neutron scattering. Although phonon data recorded at low temperatures would be more appropriate for the present purpose, only data for room temperature appear to exist in the literature.[69] The elastic model achieves better agreement with the experimentally observed vibrational modes of neutral Fe_3 (ν=180, 200 cm^{-1}) (Ref. 70) than DFT calculations.[71] Rotational constants of the clusters are estimated by calculating moments of inertia for the corresponding substructures of the body-centered cubic crystal as detailed elsewhere.[26] In all cases, the clusters are presumed to be spherical rotors. For Fe_2^+, however, the constants of the neutral dimer Fe_2, ν=300 cm^{-1} and a bond distance of 2.02 Å to calculate the rotational constant,[72] are used without further modification.

TABLE IX. Rotational constants B and vibrational modes ν for $Fe_nS_2^+$ (all values in cm^{-1}).

n	B	ν_L[a]	$\nu_{T,1}$[b]	$\nu_{T,2}$[b]
1	0.14	543	286	303
2	0.069	318	210	168
		425		277
		450		
3	0.015	148	270	127
		237	270	270
		300		270
		300		
4	0.011	138	118	118
		220	270	189
		239	270	270
		300		270
		300		

[a]Longitudinal branch.
[b]Transverse branches.

APPENDIX C: MOLECULAR PARAMETERS OF IRON–SULFUR CLUSTERS Fe_nS^+ AND $Fe_nS_2^+$

For FeS,[73] experimental values for the vibrational frequency and the bond distance to calculate the rotational constant are available, whereas for FeS_2^+,[74] Fe_2S^+, and $Fe_2S_2^+$,[13] these properties were taken from the results of quantum chemical calculations.

For larger iron-sulfur clusters, Fe_nS^+ and $Fe_nS_2^+$, the S atoms are assumed to adopt bridging positions. Such bridging geometries are observed in the complexes $[Fe_3(CO)_9S]^{2-}$ and $Fe_4(CO)_{11}S_2$ (Ref. 63) and are also supported by the thermodynamic results of this work. Hence, Fe_nS^+ and Fe_{n+1}^+ ($n=3-6$) are assumed to have similar structures. For the Fe_nS^+ clusters, three modes (the median of the longitudinal and both transverse branches) of the Fe_{n+1}^+ clusters are replaced by the three modes characteristic of S bound to a metal surface. The symmetric stretching mode of S attached to a Ni surface is known as 359 cm^{-1},[75] which allows an estimate of the frequency of the vibration parallel to the surface as 320 cm^{-1} (on the basis of the ratio observed for the different motions of O attached to Ni).[76] Scaling these frequencies by the ratio $\nu(FeS)/\nu(NiS)=0.84$ (Ref. 77) yields frequencies of 300 cm^{-1} for the longitudinal branch and 270 cm^{-1} for both of the transverse branches of iron–sulfur clusters Fe_nS^+ (Table VIII). For the $Fe_nS_2^+$ clusters, $n=2-4$, an analogous approach starting with the frequencies estimated for Fe_nS^+ is made (Table IX). The rotational constants are calculated similarly to those of bare clusters Fe_n^+, employing an averaged atom mass. In all cases, the clusters are presumed to be spherical rotors.

APPENDIX D: POLARIZABILITIES

The atomic polarizability of Fe has been determined experimentally, $\alpha(Fe)=7.5$ Å^3.[78] On the basis of several atomic metal and metal-sulfide polarizabilities, $\alpha(S)=2.90$ Å^3, $\alpha(Zn)=5.6$ Å^3,[79] $\alpha(ZnS)=9.3$ Å^3,[80] $\alpha(Cd)=7.2$ Å^3,[79] $\alpha(CdS)=10.9$ Å^3,[80] $\alpha(Hg)=5.7$ Å^3,[79] and $\alpha(HgS)=9.4$ Å^3,[80] a simple linear correlation approach suggests $\alpha(FeS)\approx 11$ Å^3. It was checked that varying the value for $\alpha(FeS)$ only very weakly affects the threshold analysis.

[1] *Iron–Sulfur Proteins*, edited by W. Lovenberg (Academic, New York, 1973–1977).
[2] *Iron–Sulfur Proteins*, edited by T. G. Spiro (Wiley, New York, 1982).
[3] H. Beinert, FASEB J. **4**, 2483 (1990).
[4] R. Cammack, *Advances in Inorganic Chemistry* (Academic, New York, 1992).
[5] D. H. Flint and R. M. Allen, Chem. Rev. **96**, 2315 (1996).
[6] N. Zhang, T. Hayase, H. Kawamata, K. Nakao, A. Nakajima, and K. Kaya, J. Chem. Phys. **104**, 3413 (1996).
[7] A. Nakajima, T. Hayase, H. Kawamata, F. Hayakawa, and K. Kaya, Chem. Phys. Lett. **280**, 381 (1997).
[8] J. N. Harvey, C. Heinemann, A. Fiedler, D. Schröder, and H. Schwarz, Chem.-Eur. J. **2**, 1230 (1996).
[9] D. Schröder, I. Kretzschmar, H. Schwarz, C. Rue, and P. B. Armentrout, Inorg. Chem. **38**, 3474 (1999).
[10] T. C. Jackson, T. J. Carlin, and B. S. Freiser, Int. J. Mass Spectrom. Ion Processes **72**, 169 (1986).
[11] T. J. McMahon, T. C. Jackson, T. J. Carlin, and B. S. Freiser, J. Am. Chem. Soc. **111**, 421 (1989).
[12] J. N. Harvey, D. Schröder, and H. Schwarz, Inorg. Chim. Acta **273**, 111 (1998).
[13] O. Hübner, Ph.D. thesis, Humboldt-Universität, Berlin, 2002.
[14] O. Hübner and J. Sauer, J. Chem. Phys. **116**, 617 (2002).
[15] Z. Yu, N. Zhang, X. Wu, Z. Gao, Q. Zhu, and F. Kong, J. Chem. Phys. **99**, 1765 (1993).
[16] J. H. El Nakat, K. J. Fisher, I. G. Dance, and G. D. Willett, Inorg. Chem. **32**, 1931 (1993).
[17] S. Bililign, C. S. Feigerle, and J. C. Miller, Appl. Surf. Sci. **127–129**, 344 (1998).
[18] R. J. P. Williams, Nature (London) **343**, 213 (1990).
[19] C. Huber and G. Wächtershäuser, Science **276**, 245 (1997).
[20] C. Huber and G. Wächtershäuser, Science **281**, 670 (1998).
[21] P. B. Armentrout, J. B. Griffin, and J. Conceição, in *Progress in Physics of Clusters*, edited by G. N. Chuev, V. D. Lakhno, and A. P. Nefedov (World Scientific, Singapore, 1999), p. 198.
[22] K. M. Ervin, Chem. Rev. **101**, 391 (2001).
[23] M. T. Rodgers and P. B. Armentrout, Mass Spectrom. Rev. **19**, 215 (2000).
[24] L. Lian, C.-X. Su, and P. B. Armentrout, J. Chem. Phys. **97**, 4072 (1992).
[25] P. B. Armentrout and B. L. Kickel, in *Organometallic Ion Chemistry*, edited by B. S. Freiser (Kluwer Academic, Dordrecht, 1996), p. 1.
[26] J. Conceição, S. K. Loh, L. Lian, and P. B. Armentrout, J. Chem. Phys. **104**, 3976 (1996).
[27] J. B. Griffin and P. B. Armentrout, J. Chem. Phys. **106**, 4448 (1997).
[28] J. B. Griffin and P. B. Armentrout, J. Chem. Phys. **107**, 5345 (1997).
[29] R. Liyanage, X.-G. Zhang, and P. B. Armentrout, J. Chem. Phys. **115**, 9747 (2001).
[30] S. K. Loh, D. A. Hales, L. Lian, and P. B. Armentrout, J. Chem. Phys. **90**, 5466 (1989).
[31] T. G. Deitz, M. A. Duncan, D. E. Powers, and R. E. Smalley, J. Chem. Phys. **74**, 6511 (1981).
[32] X.-C. Su and P. B. Armentrout, J. Chem. Phys. **99**, 6506 (1993).
[33] D. A. Hales, X.-C. Su, L. Lian, and P. B. Armentrout, J. Chem. Phys. **100**, 1049 (1994).
[34] E. Teloy and D. Gerlich, Chem. Phys. **4**, 417 (1974).
[35] D. Gerlich, Adv. Chem. Phys. **82**, 1 (1992).
[36] N. R. Daly, Rev. Sci. Instrum. **31**, 264 (1959).
[37] K. M. Ervin and P. B. Armentrout, J. Chem. Phys. **83**, 166 (1985).
[38] F. Muntean and P. B. Armentrout, J. Chem. Phys. **115**, 1213 (2001).
[39] T. S. Beyer and D. F. Swinehart, J. Assoc. Comput. Mach. **16**, 379 (1973).
[40] S. E. Stein and B. S. Rabinovitch, J. Chem. Phys. **58**, 2438 (1973).
[41] S. E. Stein and B. S. Rabinovitch, Chem. Phys. Lett. **49**, 1883 (1977).
[42] P. B. Armentrout, Int. J. Mass. Spectrom. **200**, 219 (2000).
[43] P. B. Armentrout, J. Am. Soc. Mass Spectrom. **13**, 419 (2002).
[44] R. G. Gilbert and S. C. Smith, *Theory of Unimolecular and Recombination Reactions* (Blackwell Scientific, Oxford, 1990).
[45] D. G. Truhlar, B. C. Garrett, and S. J. Klippenstein, J. Phys. Chem. **100**, 12771 (1996).
[46] K. A. Holbrook, M. J. Pilling, and S. H. Robertson, *Unimolecular Reactions*, 2nd ed. (Wiley, New York, 1996).
[47] M. T. Rodgers, K. M. Ervin, and P. B. Armentrout, J. Chem. Phys. **106**, 4499 (1997).
[48] A. A. Shvartsburg, J. H. Frederick, and K. M. Ervin, J. Chem. Phys. **104**, 8470 (1996).

[49] C. Rue, P. B. Armentrout, I. Kretzschmar, D. Schröder, and H. Schwarz, J. Phys. Chem. A **105**, 8456 (2001).
[50] J. B. Pedley, R. D. Naylor, and S. P. Kirby, *Thermochemical Data of Organic Compounds* (Chapman and Hall, London, 1986). Corrected to 0 K using $H^\circ - H^\circ(298.15\ \mathrm{K})$ values taken from Ref. 51.
[51] M. W. Chase, Jr., C. A. Davies, J. R. Downey, Jr., D. J. Frurip, R. A. McDonald, and A. N. Syverud, J. Phys. Chem. Ref. Data Suppl. **14**, 1 (1985).
[52] C. E. Moore, *Atomic Energy Levels* (National Standard Reference Data Series, National Bureau of Standards, NSRDS-NBS 35, Washington, D.C., 1971).
[53] J. Drowart, A. Pattoret, and S. Smoes, Proc. Br. Ceram. Soc. **8**, 67 (1967).
[54] J. Sugar and C. Corliss, J. Phys. Chem. Ref. Data Suppl. **14**, 1 (1985).
[55] L. S. Sunderlin, D. Wang, and R. R. Squires, J. Am. Chem. Soc. **114**, 2788 (1992).
[56] P. W. Villalta and D. G. Leopold, J. Chem. Phys. **98**, 7730 (1993).
[57] S. K. Loh, L. Lian, and P. B. Armentrout, J. Chem. Phys. **91**, 6148 (1989).
[58] C. Rue, P. B. Armentrout, I. Kretzschmar, D. Schröder, J. N. Harvey, and H. Schwarz, J. Chem. Phys. **110**, 7858 (1999).
[59] G. Herzberg, *Molecular Spectra and Molecular Structure*, reprint ed. (Krieger, Malabar, 1991), Vol. III.
[60] A. A. Shvartsburg, K. M. Ervin, and J. H. Frederick, J. Chem. Phys. **104**, 8458 (1996).
[61] J. E. Demuth, D. W. Jepsen, and P. M. Marcus, Phys. Rev. Lett. **32**, 1182 (1974).
[62] L. H. Dubois, J. Chem. Phys. **77**, 5228 (1982).
[63] H. Ogino, S. Inomata, and H. Tobita, Chem. Rev. **98**, 2093 (1998).
[64] In Ref. 28, p. 5353, Table II, $D(\mathrm{Fe}_n^+ - \mathrm{O})^a$, $n=3$, should read 5.6(0.2) instead of 4.5(0.2) eV.
[65] E. A. Rohlfing, D. M. Cox, A. Kaldor, and K. H. Johnson, J. Chem. Phys. **81**, 3846 (1984).
[66] P. Jackson, J. N. Harvey, D. Schröder, and H. Schwarz, Int. J. Mass. Spectrom. **204**, 233 (2001).
[67] N. W. Ashcroft and N. D. Mermin, *Solid State Physics* (Saunders College, Philadelphia, 1976), p. 461.
[68] G. Simmons and H. Wang, *Single Crystal Elastic Constants and Calculated Aggregate Properties: A Handbook*, 2nd ed. (MIT, Cambridge, 1971).
[69] R. Röhlsberger, W. Sturhahn, T. S. Toellner, K. W. Quast, M. Hession, M. Hu, J. Sutter, and E. E. Alp, J. Appl. Phys. **86**, 584 (1999).
[70] E. M. Nour, C. Alfaro-Franco, K. A. Gingerich, and J. Lanne, J. Chem. Phys. **86**, 4779 (1987).
[71] M. Castro and D. R. Salahub, Phys. Rev. B **49**, 11842 (1994).
[72] M. D. Morse, Chem. Rev. **86**, 1049 (1986).
[73] T. C. DeVore and H. F. Franzen, High. Temp. Sci. **7**, 220 (1975).
[74] I. Kretzschmar, *Energetics and Reactivity of the Binary Transition-Metal Sulfides of the 3rd and the 4th Row* (Shaker Verlag, Aachen, 1999).
[75] S. Andersson, Surf. Sci. **79**, 385 (1979).
[76] S. Andersson, P.-A. Karlsson, and M. Persson, Phys. Rev. Lett. **51**, 2378 (1983).
[77] C. W. Bauschlicher, Jr. and P. Maitre, Theor. Chim. Acta **90**, 189 (1995).
[78] T. M. Miller and B. Bederson, Adv. At. Mol. Phys. **13**, 1 (1977).
[79] *CRC Handbook of Chemistry and Physics*, 79th ed., edited by D. R. Lide (CRC, Boca Raton, 1998–1999).
[80] S. G. Raptis, M. G. Papadopoulos, and A. J. Sadlej, J. Chem. Phys. **111**, 7904 (1999).